scientific reports

OPEN

Towards middle-up analysis of polyclonal antibodies: subclass-specific *N*-glycosylation profiling of murine immunoglobulin G (IgG) by means of HPLC-MS

Constantin Blöchl[1], Christof Regl[1,2], Christian G. Huber[1,2], Petra Winter[3], Richard Weiss[3] & Therese Wohlschlager[1,2]✉

In recent years, advanced HPLC-MS strategies based on intact protein ("top-down") or protein subunit ("middle-up/middle-down") analysis have been implemented for the characterization of therapeutic monoclonal antibodies. Here, we assess feasibility of middle-up/middle-down analysis for polyclonal IgGs exhibiting extensive sequence variability. Specifically, we addressed IgGs from mouse, representing an important model system in immunological investigations. To obtain Fc/2 portions as conserved subunits of IgGs, we made use of the bacterial protease SpeB. For this purpose, we initially determined SpeB cleavage sites in murine IgGs. The resulting Fc/2 portions characteristic of different subclasses were subsequently analysed by ion-pair reversed-phase HPLC hyphenated to high-resolution mass spectrometry. This enabled simultaneous relative quantification of IgG subclasses and their *N*-glycosylation variants, both of which influence IgG effector functions. To assess method capabilities in an immunological context, we applied the analytical workflow to polyclonal antibodies obtained from BALB/c mice immunized with the grass pollen allergen Phl p 6. The study revealed a shift in IgG subclasses and Fc-glycosylation patterns in total and antigen-specific IgGs from different mouse cohorts, respectively. Eventually, Fc/2 characterization may reveal other protein modifications including oxidation, amino acid exchanges, and C-terminal lysine, and may thus be implemented for quality control of functional antibodies.

Emergence of novel analytical technologies has driven the development of high-performance liquid chromatography (HPLC) and mass spectrometry (MS) strategies for intact protein characterization. In contrast to conventional peptide analysis, referred to as "bottom-up" approach, intact mass determination provides information on protein integrity and on the coexistence of protein variants arising from glycosylation and other post-translational modifications (PTMs)[1]. If combined with gas-phase fragmentation in a so-called "top-down" approach, information on the amino acid sequence may be obtained. With protein variants being highly relevant in the context of biopharmaceuticals, numerous methods for the characterization of intact therapeutic monoclonal antibodies (mAbs) and Fc-fusion proteins have been described[2–9]. Alternatively, mAb subunits obtained by reduction of disulphide bonds or limited proteolysis may be analysed. The latter usually involves digestion with the IdeS protease, which has become a valuable tool for the characterization of human therapeutic mAbs[10–13]. The analytical approach is referred to as "middle-up" if protein subunit masses are determined. In case of additional gas-phase dissociation and fragment mass determination, the analysis is termed "middle-down"[1].

In contrast to monoclonal immunoglobulin G (IgG)-type antibodies, native polyclonal IgGs occurring in biological samples, e.g. serum, exhibit a near infinite number of sequence variants, which arise from their antigen-specific variable regions. IgGs generally consist of an antigen binding fragment (Fab) determining antigen

[1]Department of Biosciences, Bioanalytical Research Labs, University of Salzburg, Hellbrunner Straße 34, 5020 Salzburg, Austria. [2]Christian Doppler Laboratory for Innovative Tools for Biosimilar Characterization, University of Salzburg, Hellbrunner Straße 34, 5020 Salzburg, Austria. [3]Department of Biosciences, Division of Allergy and Immunology, University of Salzburg, Hellbrunner Straße 34, 5020 Salzburg, Austria. ✉email: therese.wohlschlager@sbg.ac.at

specificity and a crystallisable fragment (Fc) conveying effector functions to the antibody. Based on the conserved amino acid sequences of the Fc domain, IgGs are divided into subclasses, i.e. IgG1 to 3 in mice[14] and IgG1 to 4 in humans[15], which differ in their binding to Fc receptors (FcR) and hence their effector functions[16]. Structure and function of all IgG subclasses is additionally tuned by *N*-glycosylation of the Fc domain as has been observed for murine[17,18] and human[19] IgGs. Substitution of the conserved *N*-glycosylation site with extended *N*-glycans, for example, favours an open conformation of the Fc domain, while truncation of *N*-glycan structures or complete deglycosylation induces a more closed state of both murine[20] and human IgGs[21]. These structural alterations modulate IgG-mediated effector functions, e.g. antibody-dependent cellular cytotoxicity (ADCC), complement-dependent cytotoxicity (CDC), and anti-inflammatory responses in mice[22–24] and humans[23,25]. In addition to these structure–function relationships, IgG glycosylation profiles have been shown to be associated with the physiological state of an organism[26–28]. For example, changes in IgG glycosylation have been observed for various indications, including autoimmune diseases and cancer, in both humans and mouse models of human disease[29]. In the context of allergen-specific immunotherapy (AIT), induction of allergen-specific IgGs (so-called blocking IgGs) is of central importance for the clinical outcome of the therapy[30]. Blocking IgGs can inhibit IgE-mediated anaphylaxis by competing with IgE for allergen binding and by cross-linking FcεRI with the inhibitory receptor FcγRIIb. However, the effects of IgG subclass and Fc-glycosylation pattern in allergy remain unclear[31].

As antibody function is controlled via changes in both antibody subclass selection and antibody glycosylation[14,32,33], monitoring of IgG glycosylation in a subclass-specific manner may reveal fine-tuning of effector functions and provide new insights into immune regulatory processes[34]. Analysis of polyclonal IgGs with respect to subclass abundances and glycosylation patterns is conventionally based on ELISA and HPLC-MS of glycopeptides/released glycans, respectively[35–39]. With regard to glycosylation of polyclonal antibodies, site-specific information may be derived from glycopeptide data facilitating assignment of certain IgG subclasses[35,37,39,40]. Assessment of glycoform heterogeneity at the intact protein level as performed for mAbs, however, is precluded by the vast number of sequence variants. In this regard, specific proteolytic cleavage in the hinge may allow segregation of the variable Fab domain to facilitate middle-up/middle-down analysis of the conserved Fc portion as determinant of the IgG subclass. Characterization of Fc may thus enable subclass-specific Fc glycosylation monitoring of polyclonal IgGs. Similar strategies have been described for the analysis of human polyclonal IgGs in that Fc/2 obtained upon digestion with IdeS was used to determine IgG1 and IgG2 allotypes[41] and to monitor oxidation in intravenous immunoglobulin preparations (IVIG)[42].

Here, we explore the potential of middle-up/middle-down analysis for polyclonal IgGs from mouse representing the main model organism for immunological studies. Considering that the IdeS protease does not act on murine IgG1 and IgG2b isoforms, we initially sought after alternative means to obtain Fc/2 subunits of all murine IgG subclasses. Hence, we evaluated suitability of the protease SpeB, the major virulence factor of the human pathogen *Streptococcus pyogenes*. SpeB was previously shown to cleave streptococcal proteins as well as human host proteins, including IgGs[43]. In this study, we investigated activity in murine IgGs and characterized the resulting cleavage products. Indeed, all murine IgG subclasses and isotypes (1/1i, 2a/c, 2b/2bi, and 3) were amenable to SpeB proteolysis. HPLC-MS analysis of the obtained Fc/2 subunits enabled assignment of IgG subclasses and isotypes in a middle-down approach. Middle-up analysis simultaneously provided quantitative information on IgG subclasses and their glycosylation variants. Finally, we demonstrate capabilities of the described workflow in a pilot study involving the analysis of polyclonal IgGs from serum of BALB/c mice immunized with timothy grass pollen allergen Phl p 6[44]. Our approach provides global information on IgG subclass abundances and their respective glycoforms and paves the way towards the characterization of polyclonal IgG proteoforms.

Results and discussion

Analytical strategy. Inspired by recent advances in the characterization of therapeutic mAbs at the subunit level, we set out to establish a middle-up workflow for Fc-glycosylation analysis in polyclonal murine IgGs. Specifically, we aimed at the analysis of Fc/2 as the determinant for IgG subclasses (see Fig. 1). To this end, we assessed the applicability of the bacterial protease SpeB to cleave polyclonal mouse IgGs of all subclasses within the hinge region (Fig. 1a,b). Digestion with SpeB was carried out under reducing conditions to keep the reactive cysteine of the protease in its active, reduced form. Moreover, SpeB was found to cleave human IgGs only if interchain disulphide bonds in the hinge region of the substrate were reduced[45]. Cleavage of murine IgGs with SpeB under reducing conditions yielded three species of IgG subunits, all approximately 25 kDa in size: light chain (LC), N-terminal part (Fd´), and C-terminal part (Fc/2) of the heavy chain (HC). Variable regions are located in LC and Fd′, whereas sequence variability of the glycosylated Fc/2 subunit is limited. In fact, each IgG subclass comprises a characteristic Fc/2 portion defined by a conserved amino acid sequence. Taking advantage of these well-defined sequence variants, we apply ion-pair reversed-phase (IP-RP)-HPLC to separate Fc/2 subunits of different IgG subclasses (Fig. 1c). Noteworthy, LC and Fd′ portions do not interfere with the analysis, as they are chromatographically separated from Fc/2 subunits. Hyphenation to high-resolution Orbitrap mass spectrometry provides qualitative and quantitative information on Fc/2 glycosylation variants (Fig. 1d). Data evaluation is performed using established software tools as described in the methods section.

Determination of SpeB cleavage products in murine IgG subclasses. In order to obtain Fc/2 subunits of all IgG subclasses described in mice, we explored the proteolytic properties of the cysteine protease SpeB. While rather loose sequence specificity was described for SpeB, cleavage is thought to be largely determined by site accessibility and hence the three-dimensional structure of the protein substrate[43,46,47]. Accordingly, SpeB preferentially cleaves human IgGs within the exposed hinge region, thereby generating free Fc/2 subunits[43]. As the cleavage sites in murine IgGs were unknown, we initially set out to identify the proteolytic products resulting from SpeB cleavage of HC portions from different IgG subclasses. For this purpose we used monoclonal

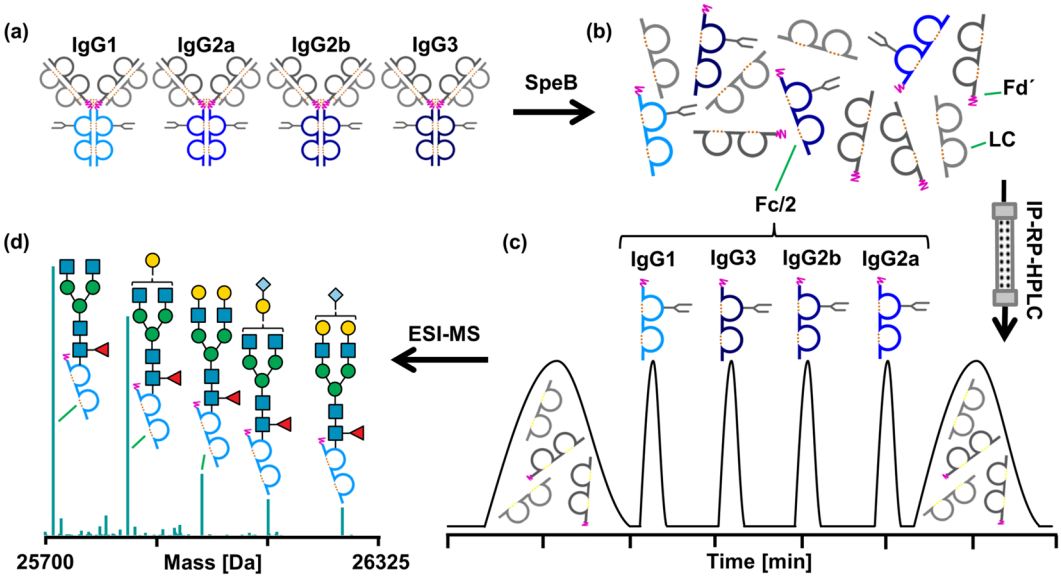

Figure 1. Schematic workflow for Fc/2 subunit characterization of polyclonal murine IgGs. (**a**) A mixture of affinity-purified polyclonal murine IgGs of different subclasses is digested with SpeB under reducing conditions. (**b**) Proteolytic cleavage in the hinge region (pink) generates LC (light grey), Fd′ (dark grey) and Fc/2 (blue) subunits. (**c**) IP-RP-HPLC of IgG subunits facilitates separation of Fc/2 portions in a subclass-specific way. (**d**) Glycoforms are identified for IgG subclasses based on mass spectra of Fc/2.

BALB/c		C57BL/6		mAb		SpeB cleavage sites	
Subclass	Uniprot ID	Subclass	Uniprot ID	Subclass	Uniprot ID	Main site	Minor site
IgG1	P01868[a]	IgG1i	A0A075B5P4	IgG1	P01868[a]	PCIC|TVPE	CKPC|ICTV
IgG2a	P01863	–	–	IgG2a	P01863	PPCK|CPAP	PAPN|LLGG
IgG2b	P01867	IgG2bi	A0A075B5P3	IgG2b	P01867	ECHK|CPAP	KECH|KCPA
–	–	IgG2c	A0A0A6YY53	–	–	CPPC|AAPD	PPCA|APDL
–	–	–	–	IgG3	P03987	TPPG|SSCP	PKPS|TPPG

Table 1. Constant HC regions and SpeB cleavage sites identified in mouse IgGs from different sources. [a]Two amino acid exchanges were detected with respect to the Uniprot entry.

mouse IgGs, i.e. IgG1, IgG2a, IgG2b and IgG3, as well as polyclonal IgGs of two commonly used inbred mouse strains, BALB/c and C57BL/6. The former mouse strain comprises IgG1, IgG2a, IgG2b and IgG3 subclasses, while C57BL/6 mice feature IgG1i, IgG2c, IgG2bi and IgG3, respectively[38]. Employing protein G affinity chromatography, we obtained mixtures of polyclonal IgGs from the serum of mouse individuals of these strains. Monoclonal antibodies as well as polyclonal IgGs were digested with SpeB for 3 h at 37 °C in the presence of L-cysteine. The generated subunits were then analysed by IP-RP-HPLC-MS, applying full MS/all ion fragmentation (AIF) mode (Supplementary Fig. S-1). HC cleavage products were subsequently determined as follows: the amino acid sequence of the HC was identified by matching y-ions (C-terminal fragments) to a candidate list of Uniprot entries; the cleavage site was localised in the identified sequence based on the experimental mass of the cleavage product; the amino acid sequence of the assigned cleavage product was verified by b-ions (N-terminal fragments). Employing this combination of middle-up and middle-down analysis, IgG subclasses from C57BL/6 could be associated with the following accession numbers: IgG1i (A0A075B5P4), IgG2bi (A0A075B5P3) and IgG2c (A0A0A6YY53). In BALB/c mice, IgG1 (P01868), IgG2a (P01863) and IgG2b (P01867) were assigned (Table 1, Supplementary Fig. S-2). IgG1 from this mouse strain corresponded to a sequence variant of the P01868 Uniprot entry comprising two amino acid exchanges (both N to D). This previously described variant was additionally confirmed by peptide analysis (Supplementary Fig. S-3)[48]. IgG3 was not detected in SpeB digests of polyclonal antibodies, which may be due to the low abundance of this subclass in serum or due to protein precipitation upon formation of cryoglobulins[49,50].

With regard to SpeB induced proteolysis, a main and a minor cleavage site were identified for HC constant regions of each IgG subclass under the applied conditions (Table 1). In accordance with previous reports, the identified cleavage sites are mainly located in unstructured, proline-rich regions, such as the hinge. The resulting C-terminal cleavage products of polyclonal and monoclonal IgGs comprising the glycosylated Fc/2 subunit are

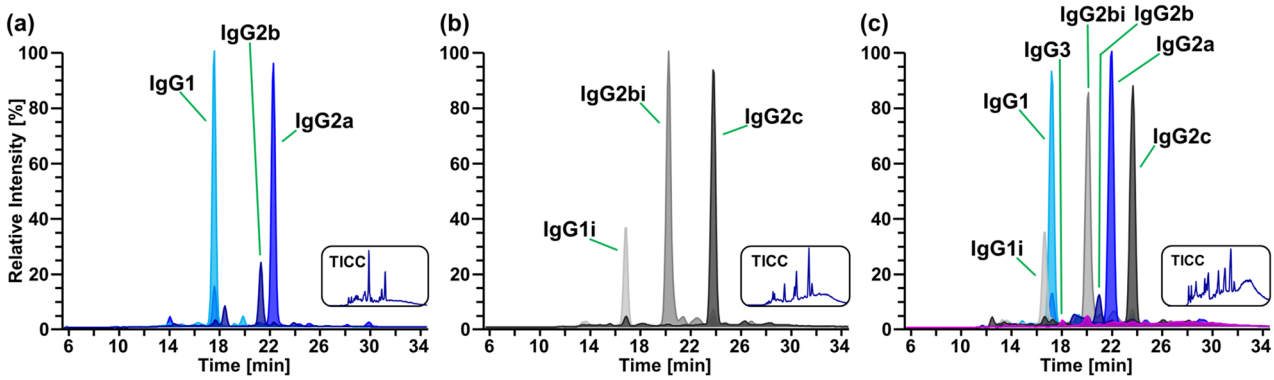

Figure 2. Separation of Fc/2 subunits in polyclonal IgGs as exemplified by XICCs for the respective G1F glycoform. Fc/2 derived from ploycloncal IgGs of (**a**) BALB/c and (**b**) C57BL/6 mice, respectively, and (**c**) a mixture from both mouse strains spiked with monoclonal IgG3 were separated. Peaks are labelled according to the IgG subclass of the underlying Fc/2 subunit. Colour-coded XICCs represent the sum of signals considering several charge states of the G1F glycoform of the respective IgG subclass. Details are provided in the Experimental Section and as Supplementary Excel file. The corresponding total ion current chromatograms (TICCs) are shown as insets.

listed in Supplementary Table S-1. Based on the identified Fc/2 subunits, we generated extracted ion current chromatograms (XICCs) to assess chromatographic separation of the different cleavage products: indeed, Fc/2 subunits obtained from polyclonal IgGs could be separated in a subclass-specific manner by means of IP-RP-HPLC (Fig. 2a,b). Hence, relative abundances of main and minor C-terminal cleavage products could be determined based on peak areas obtained from the corresponding XICCs (Supplementary Table S-1, Supplementary Fig. S-4).

In order to further assess the capabilities of the chromatographic method, we analysed a mixture of all described murine IgG subclasses and isotypes, i.e. a combination of polyclonal IgGs from C57BL/6 and BALB/c spiked with monoclonal IgG3. Indeed, Fc/2 subunits from all seven murine IgG subclasses and isotypes could be separated and identified (Fig. 2c). Intriguingly, Fc/2 of even closely related isotypes was readily separated as demonstrated for IgG1 and IgG1i differing in only three out of 213 amino acids. Chromatographic separation is a prerequisite for quantitative analysis of Fc/2 subunits based on XICCs as peak areas may be biased upon co-elution.

Relative quantification of IgG subclasses. IgG subclasses may be quantified based on relative abundances of the respective Fc/2 subunits taking into account all identified glycoforms (see "Identification and relative quantification of Fc/2 glycoforms"). For this purpose, we determined peak areas in corresponding XICCs and corrected relative abundances of Fc/2 for minor cleavage products (Supplementary Table S-1, Supplementary Excel file). The resulting IgG subclass abundance profiles obtained for a BALB/c and a C57BL/6 mouse individual are shown in Supplementary Fig. S-5. Intriguingly, IgG1 predominated in the BALB/c mouse, whereas higher levels of IgG2c (homologous to IgG2a in BALB/c) and IgG2bi were observed in the C57BL/6 individual. This is in accordance with the default immune polarization of the two prototypical mouse strains, arising from T helper type 2 (Th2) and T helper type (Th1) dominated immune responses, respectively[51]. Subclass quantification of several mouse individuals was performed in the course of a vaccination study in BALB/c mice (see below).

In the investigated purified polyclonal antibodies, Fc/2 subunits of IgG3 were not detected, most likely due to the low abundance of this IgG subclass. In principle, the detection of this subclass is possible as demonstrated by spiking a mixture of polyclonal IgGs with monoclonal IgG3 (Fig. 2c). Downscaling of the applied HPLC-MS setup to the nanoscale may increase sensitivity to enable routine detection of IgG3.

The here described HPLC-MS based approach provides IgG subclass profiles enabling direct comparison of different subclasses within a mouse individual. Inherent to mass spectrometric detection, response factors of Fc/2 from different IgG subclasses and their glycoforms may vary. However, we expect the response factor to be less affected by a particular molecular difference in case of the protein subunit as compared to the glycopeptide. With respect to total IgGs obtained by protein G affinity chromatography, subtle differences in affinity may affect subclass quantification, even though roughly comparable affinities have been reported for all murine IgG subclasses[52]. Employing the affinity matrix in excess may counteract this potential bias. On the other hand, our HPLC-MS based workflow is potentially favourable for subclass quantification of antigen-specific IgGs. The latter conventionally involves direct ELISA, which may be biased by different affinities of detection antibodies when comparing individual subclasses. Middle-up analysis therefore represents an attractive alternative, e.g. for the determination of immunologically relevant IgG1/IgG2a ratios[53].

Identification and relative quantification of Fc/2 glycoforms. Upon subclass-specific separation and identification of Fc/2 subunits from polyclonal IgGs of BALB/c mice, we assessed *N*-glycosylation variants of Fc/2 based on full scan mass spectra in a middle-up approach. Taking into account the mass of the amino acid sequence as well as the mass of potential *N*-glycan structures reported in the literature[38] (Supplementary

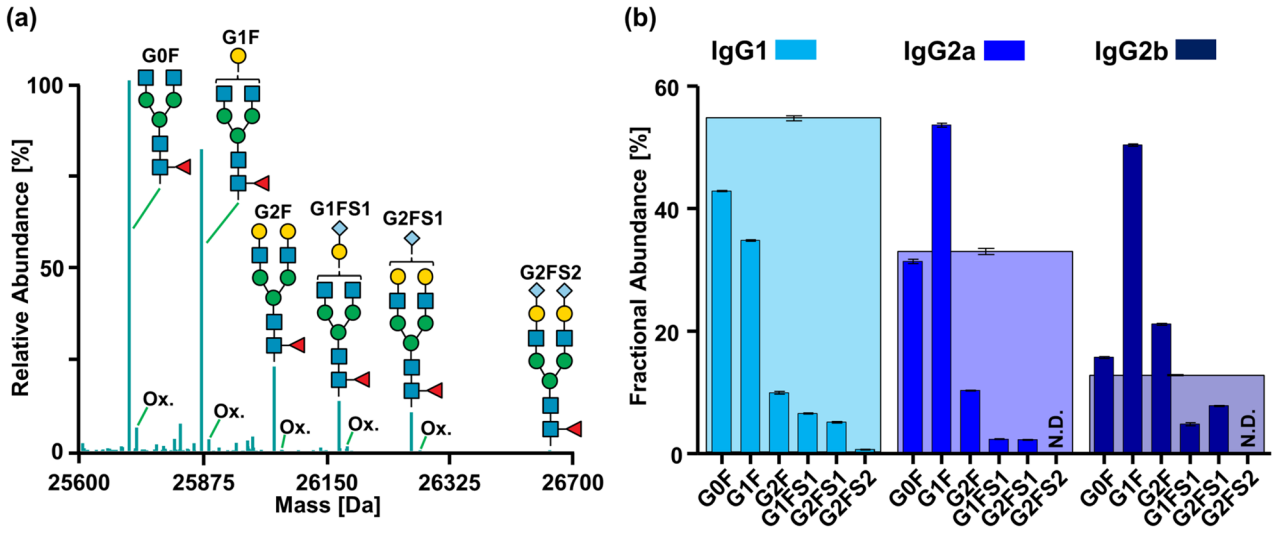

Figure 3. Fc/2-based subclass and glycoform quantification of polyclonal IgGs from a BALB/c mouse individual. (**a**) Deconvoluted mass spectrum of Fc/2 from IgG1 with assigned *N*-glycan structures and oxidation variants (Ox.). The signal annotated as G2F may partially arise from isobaric αG2F comprising α-gal; the peak assigned as oxidised G1FS1 may partially arise from the αG3F glycoform (see main text). (**b**) Fractional abundances of IgG subclasses (wide bars) and their respective *N*-glycoforms (narrow bars). Abbreviations for *N*-glycans correspond to structures shown in (**a**). Relative abundances were obtained from XICCs of Fc/2 subunits (Supplementary Excel file). Mean values are based on three technical replicates; error bars indicate standard deviations. Raw spectra are shown in Supplementary Fig. S-6.

Table S-2), glycoforms were assigned using the MoFi software[54]. Six *N*-glycan structures of the biantennary, complex type were identified for Fc/2 from IgG1 (Fig. 3a and Supplementary Fig. S-6). The assigned structures all comprise core-fucose residues and are substituted with up to two *N*-glycolylneuraminic acid (Neu5Gc) moieties. The same glycans, however at different abundances, were identified for Fc/2 from IgG2a and IgG2b (Supplementary Fig. S-6). In addition to masses arising from different glycoforms, we observed a series of signals shifted by + 16 Da with respect to the detected glycoforms. These masses may be attributed to oxidation variants, which is further supported by the detection of oxidised tryptic peptides within Fc/2 (Fig. 3a and Supplementary Fig. S-7).

Isomeric glycoforms, e.g. resulting from different glycosidic linkages, cannot be distinguished with our method and require complementary strategies involving released glycan or glycopeptide analysis[55]. Specifically, this concerns *N*-glycoforms comprising α-gal structures (galactose-α-1,3-galactose), which have been reported to occur in murine IgGs in small amounts and were hence included in our *N*-glycan library (Supplementary Table S-2)[28,38]. However, isobaricity of the αG2F structure (comprising α-gal) and the more abundant G2F structure precluded unambiguous assignment of the corresponding peaks. Furthermore, Fc/2 comprising an αG3F structure could not be distinguished from oxidised Fc/2 substituted with G1FS1 as the monoisotopic masses of these variants only differed by approximately one Dalton. For simplicity, α-gal structures as minor contributors of the respective signals are not shown in the corresponding figures. Other isomeric glycan structures that cannot be discerned by the described middle-up approach include 3-arm and 6-arm isomers of G1F and G1FS1, respectively. The problem of isobaricity also concerns afucosylated glycoforms and oxidation variants of the corresponding fucosylated glycoforms lacking a hexose. However, we did not detect the afucosylated G0 glycoform for which no such isobaric variant exists, thus enabling unambiguous assignment of this specific peak.

For relative quantification of IgG subclasses and their *N*-glycoforms (Fig. 3b), peak areas were obtained from XICCs of the identified glycoforms in a subclass-specific manner. In IgG1, the non-galactosylated G0F structure predominated whereas the *N*-glycan extended with one galactose residue (G1F) was most abundant in both IgG2a and IgG2b (Fig. 3b). The here described subclass-specific differences of IgG *N*-glycan profiles in naive BALB/c mice are in line with previous reports on murine IgG glycosylation[38,39,56]. In addition to polyclonal IgGs, we analysed monoclonal antibodies of different subclasses applying the above described middle-up approach. Mass spectra revealed additional PTMs in these IgGs: based on characteristic mass shifts, oxidation variants of Fc/2 glycoforms were detected in all analysed mAbs and are exemplified for monoclonal IgG1 and IgG2b in Supplementary Fig. S-8. Moreover, we observed Fc/2 variants in monoclonal IgG1 and IgG2b comprising a mass shift of + 128 Da, which may be attributed to incomplete processing of the C-terminal lysine residue. Detection of lysine variants was even possible if main and minor cleavage products differed by one N-terminal lysine residue as demonstrated for IgG2b (Supplementary Fig. S-8). Simultaneous determination of Fc/2 glycosylation and oxidation variants may be of relevance in quality assessment of functional mouse IgGs. Indeed, both modifications impact downstream effector functions, e.g. oxidised mAbs display decreased affinity to Fcγ receptors[57]. Thus, profiling of Fc/2 glycosylation and oxidation variants of murine mAbs may be especially relevant for

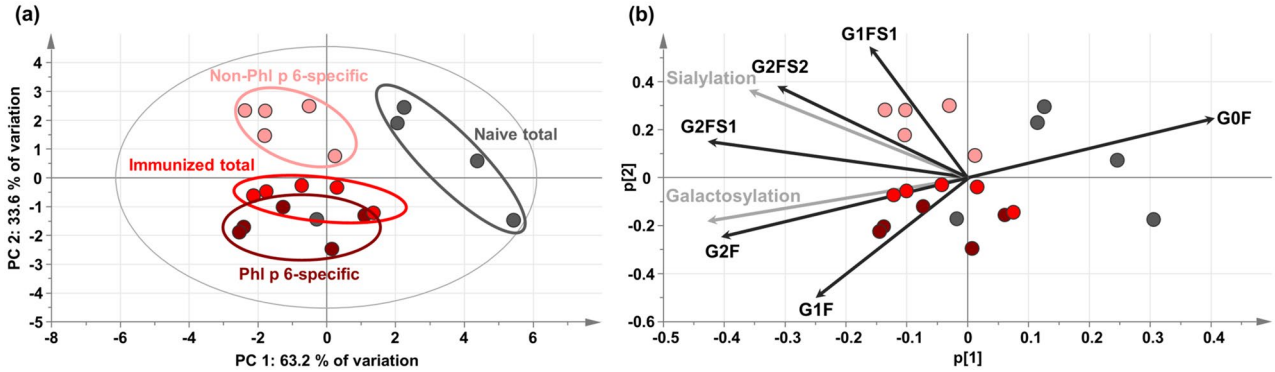

Figure 4. Principal component analysis (PCA) of IgG1 *N*-glycosylation profiles in naive BALB/c mice and BALB/c vaccinated with Phl p 6 in absence of adjuvant. (**a**) Score plot of IgG1 glycan profiles in total IgG from naive mice (grey) and in three fractions of Phl p 6 vaccinated mice, i.e. total IgG1 (red), Phl p 6-specific IgG1 (dark red) and non-Phl p 6-specific IgG1 (light red). Each dot represents the glycan profile of a mouse individual obtained as mean of three technical replicates. (**b**) Loading plot showing the contribution of the individual *N*-glycan structures (black) and traits (grey); sialylation and galactosylation refer to the summed weighted abundances of all sialylated and galactosylated structures, respectively, as previously described[62]. Fractional glycoform abundances are listed in the Supplementary Excel file.

immunological studies in mice using these mAbs as functional tools, e.g. for in vivo depletion of specific cell types via ADCC and complement-dependent cytotoxicity.

In terms of closely related IgG isotypes, our middle-up approach provides new means to fully assess isotype-specific glycosylation patterns, which were not amenable by conventional bottom-up analysis. While tryptic glycopeptides from murine IgGs allow discrimination of subclasses 1, 2 and 3, these specific peptides are isobaric for the four IgG2 isotypes. Although tryptic glycopeptides of IgG2a/2c may be chromatographically separated from those of IgG2b/2bi, discrimination of IgG2a from IgG2c and IgG2b from IgG2bi is not possible because of identical tryptic glycopeptides[39]. Middle-up analysis of polyclonal IgGs circumvents these restrictions and reveals glycosylation profiles with unlimited subclass specificity. This is especially relevant for immunological studies performed in outbred mouse stocks, e.g. Swiss Webster and CD-1, in which IgG2 isotypes may co-occur[58].

Subclass-specific analysis of Fc/2 from BALB/c mice upon vaccination with Phl p 6. In order to assess applicability of the described middle-up approach in an immunological context, we set out to determine the effects of a plant allergen on IgG subclass and glycosylation abundances in mice. Subclass distribution induced by allergen-specific immunotherapy is of clinical importance, as IgG subclasses seem to functionally differ in their allergen blocking capacity[59]. Here, we studied the immunological response of BALB/c mice to vaccination with Phl p 6, a protein allergen from timothy grass pollen (*Phleum pratense*)[44]. Four cohorts of five mouse individuals each were analysed: (i) naive, (ii) Phl p 6 vaccinated, (iii) Phl p 6 co-administered with the Th2 adjuvant aluminumhydroxid (alum), and (iv) Phl p 6 co-administered with the Th1 adjuvant CpG-ODN1826 (CpG). Polyclonal IgGs were obtained from each mouse individual by protein G affinity chromatography. Additionally, antigen-specific IgGs of the three vaccinated mouse groups were affinity-purified from the obtained total IgGs using immobilized Phl p 6. All three fractions, i.e. total, antigen-specific and non-antigen-specific IgGs, were subjected to middle-up analysis for comprehensive characterization of IgG subclass abundances and glycosylation (Supplementary Fig. S-9). Indeed, relative abundances of IgG subclasses drastically changed in response to vaccination with Phl p 6 (Supplementary Fig. S-10). Immunization with Phl p 6 exclusively induced IgG1 antibodies resulting in a significant increase in the relative abundance of total IgG1. Similarly, vaccination with Phl p 6 and the adjuvant alum induced antigen-specific IgG1 and shifted the ratio of total IgG1 to IgG2a/b towards IgG1. In contrast, higher levels of antigen-specific IgG2a and IgG2b were observed upon co-administration of Phl p 6 and the adjuvant CpG. This is in accordance with non-methylated CpG motifs in bacterial or viral DNA promoting Th1 immunity resulting in a class switch to IgG2a[60]. Intriguingly, relative subclass abundances of non-antigen-specific IgGs differed from those of total IgGs in naive mice only if adjuvants was co-administered with Phl p 6. This effect may be attributed to bystander activation of non-Phl p 6 Th cells accompanied by a class-switch in B cells[61].

In order to assess the effect of vaccination on *N*-glycosylation profiles, we compared relative glycoform abundances of IgGs from the different mouse cohorts. In case of total IgG1, we observed increased levels of the G1F glycoform and decreased levels of the G0F variant in vaccinated mouse cohorts compared to naive mice, independent of the adjuvants (Supplementary Fig. S-11). In contrast, relative glycoform abundances of total IgG2a and IgG2b were not affected by vaccination as compared to untreated mice. Although absolute changes in glycoform abundances were low, they may be relevant in terms of effector functions. To comprehensively compare IgG1 glycosylation patterns of naive mice and the cohort of Phl p 6-treated mice in absence of adjuvant, we generated integrated multivariate glycan profiles using principle component analysis (PCA). Indeed, glycosylation patterns of total IgG1 clustered into groups of immunized and naive mice (Fig. 4a). One mouse of the naive cohort clustered with the immunized group, indicating an ongoing immune reaction, which may

occur in specific-pathogen free (SPF) animals. This is supported by elevated levels of total IgG purified from this mouse individual (data not shown). Furthermore, Fc/2 *N*-glycoform abundances of the outlier resemble that of vaccinated mice rather than the naive mouse individuals (Supplementary Fig. S-12).

We next compared glycosylation patterns of Phl p 6-specific IgG1 and the remaining fraction of non-Phl p 6-specific IgG1 in immunized mice. Clustering of these two fractions in PCA revealed distinct glycan profiles of antigen-specific and non-antigen-specific IgG1. Intriguingly, all three fractions of the immunized cohort separated from total IgG1 of naive mice in PCA. As illustrated by the corresponding loading plot, the two mouse cohorts mainly differed in their galactosylation levels (Fig. 4b). Separation of Phl p 6-specific and non-Phl p 6-specific IgG1 of the vaccinated cohort can primarily be attributed to differences in the levels of G1F and G1FS1 glycoforms (Fig. 4b). Furthermore, an increase in G1F and G2F structures was observed for Phl p 6-specific IgG1 as compared to non-Phl p 6-specific IgG1. Interestingly, elevated galactosylation levels have been described for antigen-specific IgGs upon immunization with influenza or tetanus vaccine in humans[62].

With respect to AIT, low-galactosylated murine IgG1 has been recently shown to be slightly more efficient in allergen inhibition, potentially due to its higher affinity for FcγRIIb. Moreover, IgG-mediated side effects of AIT were dependent on IgG subclass and glycosylation pattern. The authors conclude that AIT protocols should aim at promoting to induce sialylated human IgG4 (functionally equivalent to murine IgG1) to limit therapy-induced side effects[31]. Comprehensive subclass specific *N*-glycosylation profiling may be applied to study IgG glycosylation in the context of hypersensitivity reactions which are partly governed by IgG binding affinities to different Fcγ receptors[63]. Furthermore, mouse models for autoimmune diseases, e.g. Sjögren's syndrome or rheumatoid arthritis, would be compelling topics to be tackled by global Fc/2 profiling[64,65].

For this vaccination study, we sacrificed mouse individuals to obtain sufficient serum (400 µL) for purification and analysis of antigen-specific IgG. Significantly less material is required for the analysis of total IgGs. Considering titers of total IgGs in murine serum (approx. 1–5 mg mL^{-1})[66] and low sample amounts required for analysis (3 µg per HPLC-MS run), also longitudinal mouse studies employing blood draw from live animals are readily feasible with our approach. Furthermore, implementation of nanoHPLC-MS may facilitate analysis of even smaller sample amounts in the future.

Conclusion

Top-down and middle-up/middle-down analytical strategies are widely applied for monoclonal antibody characterization. Although highly relevant in immunological studies, analysis of their native counterparts, i.e. polyclonal IgGs, is challenged by immense molecular heterogeneity arising from sequence variability. In this study, we devised an analytical strategy for the characterization of the functionally important Fc subunit in murine IgGs by combining middle-up and middle-down approaches. Sequence heterogeneity could be tackled by dissociating conserved Fc regions from variable domains using the protease SpeB. In summary, the described workflow accomplishes global analysis of polyclonal murine IgGs with respect to subclass abundances (including closely related isotypes), glycosylation profiles and occurrence of other modifications, e.g. oxidation and lysine variants. This comprehensive set of information may be obtained in a single analysis involving swift sample preparation, standard HPLC-MS analysis, and straightforward data evaluation. Our approach therefore represents an attractive extension to the toolbox of existing bottom-up strategies. In the future, global IgG subclass quantification and *N*-glycoform profiling may be implemented for human polyclonal antibodies at the level of Fc/2 subunits, e.g. for monitoring of IgG subclasses and allotypes in human vaccination studies.

Methods

Materials. Acetonitrile (ACN, ≥ 99.9%) was purchased from VWR International (Vienna, Austria). Ammonium hexa-fluorophosphate (AHFP, 99.99%), trifluoroacetic acid (TFA, ≥ 99.0%), tris(2-carboxyethyl)phosphine (TCEP, ≥ 98.0%), iodoacetamide (IAA, ≥ 99.0%), formic acid (FA, 98.0–100%), L-cysteine HCl (≥ 99.0%), glycine (≥ 99%), sodium chloride (NaCl, ≥ 99.5%), sodium phosphate monobasic (≥ 99.0%), and Gibco DPBS without calcium and magnesium were obtained from Sigma-Aldrich (Vienna, Austria). Ammonium acetate (≥ 98.0%), ammonia (25% in H_2O), acetic acid (≥ 98.5%), ethanol (≥ 99.5%), and sodium hydrogencarbonate ($NaHCO_3$, ≥ 99.5%) were purchased from Merck (Darmstadt, Germany). Tris(hydroxymethyl)amino-methane (TRIS, > 99.9%) and Alu-Gel-S (alum) were obtained from Serva (Heidelberg, Germany). Deionised water was obtained from a MilliQ Integral 3 instrument (Millipore, Billerica, MA, USA). Ab Spin Trap columns (immobilized protein G) and NHS-activated sepharose 4 fast flow were purchased from GE Healthcare Life Sciences (Buckinghamshire, UK). Vivaspin 500 50 kDa MWCO filters were purchased from Sartorius (Göttingen, Germany). Corning Costar Spin-X centrifuge tube filters were obtained from Corning Inc. (Corning, NY, USA). The adjuvant CpG-ODN1826 with phosophothioate backbone (CpG) was purchased from Eurofins Genomics (Ebersberg, Germany). The allergen Phl p 6.0101 (henceforth named Phl p 6) was recombinantly expressed in *Escherichia coli*. Monoclonal murine IgG2a (cat. no. 21380071) and IgG3 (cat. no. 21810201) were purchased from ImmunoTools GmbH (Friesoythe, Germany). SpeB (Streptococcal pyrogenic exotoxin B, FabULOUS, product number A0-PU1-020) was a kind gift from Genovis AB (Lund, Sweden). Hybridoma supernatant containing monoclonal murine IgG1 and IgG2b were kindly provided by Peter Hammerl (Department of Biosciences, University of Salzburg, Austria). Sequencing grade modified Trypsin was obtained from Promega, Madison, WI, USA.

Vaccination of BALB/c mice. Female, 6–10 week-old BALB/c and C57BL/6 mice were obtained from Janvier Labs (Le Genest St. Isle, France) and maintained at the animal facility of the University of Salzburg according to local guidelines for animal care. In order to assess changes in Fc-glycosylation upon a vaccination stimulus, four cohorts of BALB/c mice (n = 5) were investigated: (i) a naive group, (ii) a Phl p 6 vaccinated group,

and two groups vaccinated with Phl p 6 in the presence of the adjuvant (iii) alum or (iv) CpG, respectively. All treated cohorts were vaccinated three times in a two week interval with 10 µg of Phl p 6 in 200 µl of PBS subcutaneously either without adjuvant, or together with 50 µg of CpG or adsorbed to 50% alum. Two weeks after the final vaccination all mice were anaesthetised by intraperitoneal injection of 100 mg kg^{-1} ketamine, 3 mg kg^{-1} xylazine, and 3 mg kg^{-1} acepromazine and exsanguinated from the retro-orbital sinus by removal of the eye. While still under anaesthesia, mice were sacrificed by cervical dislocation. The blood was allowed to clot for 1.0 h at 21 °C and was subsequently centrifuged to obtain individual serum samples. These samples were sterile-filtered using 0.45 µm filters and stored at − 20 °C until further purification. Animal experiments were approved by the Austrian Ministry of Science (permit number: BMWF-66-012/0024-II/3b/2016).

Purification of polyclonal IgGs from mouse serum. Serum samples were obtained from BALB/c and C57BL/6 mouse individuals for purification of IgGs. For this purpose, protein G columns were equilibrated five times with 400 µL of 20 mmol L^{-1} of sodium phosphate buffer (pH 7.0). Four hundred µL of serum were diluted 1:2 with 20 mmol L^{-1} sodium phosphate buffer (pH 7.0), loaded onto the spin column and incubated for 1.0 h at 21 °C on an overhead rotator. The resin was washed five times with 400 µL of 20 mmol L^{-1} sodium phosphate buffer (pH 7.0) and bound IgGs were eluted upon incubation with 300 µL of 100 mmol L^{-1} glycine buffer (pH 2.5) for 15 min at 21 °C on an overhead rotator. The eluate was immediately neutralized by addition of 33 µL of 1.0 mol L^{-1} TRIS-HCl buffer (pH 8.0). The elution step was repeated twice; eluates were pooled and desalted using a 50 kDa MWCO filter according to manufacturer's instructions. Purified IgGs were diluted in 175 mmol L^{-1} ammonium acetate (pH 6.85) to a concentration of 1.0 mg ml^{-1} for further analysis. IgG concentration was determined at 280 nm using a nanophotometer (model P330, Implen GmbH, München, Germany).

Purification of Phl p 6-specific antibodies. Antigen-specific IgGs were purified by affinity chromatography using Phl p 6-sepharose beads. For this purpose, Phl p 6 was linked to NHS-activated sepharose according to manufacturer´s instructions. Coupling was performed in 2 mmol L^{-1} sodium phosphate buffer, pH 7.4 at 4.0 °C on an overhead rotator for 19 h. Residual NHS-groups were blocked with 100 mmol L^{-1} TRIS-HCl buffer (pH 8.5) for 4.0 h at 4.0 °C while rotating. Phl p 6-sepharose beads were stored in 20% (*v/v*) ethanol solution at 4 °C until use. For purification of antigen-specific IgGs, a column was prepared by equilibrating 250 µL of Phl p 6 resin in spin filters five times with 400 µL of PBS (pH 7.4). Protein G-purified total IgGs were diluted 1:2 (*v/v*) with PBS (pH 7.4), mixed with the equilibrated beads and incubated for 2 h at 21 °C on an overhead rotator. After washing the resin five times with 400 µL of PBS (pH 7.4), antigen-specific IgGs were eluted, buffer exchanged and diluted as described above.

Sample preparation. For SpeB proteolysis, monoclonal or polyclonal IgGs were diluted in 175 mmol L^{-1} ammonium acetate to a concentration of 0.3 mg mL^{-1} and supplemented with 50 mmol L^{-1} L-cysteine. Digestion with SpeB was performed at an enzyme to substrate ratio of 2 U μg^{-1} for 3.0 h at 37 °C while shaking at 850 rpm. Samples were subjected to HPLC-MS analysis without further purification. For analysis of tryptic peptides, protein G-purified polyclonal IgGs from BALB/c were reduced with 5 mmol L^{-1} TCEP for 15 min at 60 °C in 175 mmol L^{-1} ammonium acetate at 0.1 mg mL^{-1} and alkylated with 20 mmol L^{-1} IAA for 30 min at 22 °C in the dark. Tryptic digestion was performed at a substrate to enzyme ratio of 50:1 (*w/w*) for 3.0 h at 37 °C.

High-performance liquid chromatography (HPLC). Chromatographic separation was carried out on a capillary HPLC instrument (UltiMate U3000 RSLC, Thermo Fisher Scientific, Germering, Germany). SpeB digests were separated on an AdvanceBio Diphenyl column featuring superficially porous particles (150 × 2.1 mm i.d., 3.5 µm particle size, 450 Å pore size, Agilent, Santa Clara, CA, USA) at a flow rate of 200 µL min^{-1} and a column oven temperature of 80 °C. Ten microliters of sample [0.3 mg mL^{-1}] were injected using in-line split-loop mode. A linear gradient of mobile phase solutions A (H_2O + 0.050% TFA) and B (ACN + 0.050% TFA) was applied as follows: 20.0% B for 5.0 min, 27.5%–40.0% B in 30 min, 80.0% B for 5.0 min, and 20.0% B for 20 min. UV-detection was carried out at 214 nm using a 1.4 µL flow cell. Tryptic peptides were analysed using a Hypersil GOLD aQ C18 column (100 × 1.0 mm i.d., 1.9 µm particle size, 175 Å pore size, Thermo Fisher Scientific, Sunnyvale, CA, USA) at a flow rate of 100 µL min^{-1} and a column oven temperature of 50 °C applying the following gradient: mobile phase A (H_2O + 0.10% FA), mobile phase B (ACN + 0.10% FA); 2.0% B for 5 min, 2.0–12.0% B in 5 min, 12.0–45.0% B in 40 min, 80% B for 5 min, and 2.0% B for 25 min. Ten microliters of sample [0.1 mg mL^{-1}] were injected using in-line split-loop mode.

Mass spectrometry (MS). SpeB digests were analysed on a Thermo Scientific QExactive benchtop quadrupole-Orbitrap mass spectrometer equipped with an Ion Max source with a heated electrospray ionisation (HESI) probe, both from Thermo Fisher Scientific (Bremen, Germany), and an MXT715-000-MX Series II Switching Valve (IDEX Health & Science LLC, Oak Harbor, WA, USA). Mass spectrometric data were acquired similar to a previous study[11]. Specifically, the following instrument settings were used: source heater temperature of 250 °C, spray voltage of 3.5 kV, sheath gas flow of 30 arbitrary units, auxiliary gas flow of 10 arbitrary units, capillary temperature of 320 °C, in-source collision-induced dissociation (IS-CID) of 0.0 eV, S-lens RF level of 80.0, AGC target of 3e6 at *m/z* of 1500–3000 with a maximum injection time of 200 ms, resolution of 140,000 at 200 *m/z*, and averaging of 10 microscans. MS/MS was carried out in three runs applying all ion fragmentation (AIF) in the higher-energy collisional dissociation (HCD) cell at normalized collision energy (NCE) settings of 18.0, 20.0, and 22.0, respectively, within a scan range of *m/z* 500–3000 (corresponding to 63, 70, and 77 eV collision energy for a singly charged ion at *m/z* 2000), and a resolution setting of 140,000 at *m/z* 200. MS analysis of tryptic peptides was performed on a Thermo Scientific Q Exactive Plus benchtop quadrupole-Orbitrap mass spectrometer

equipped with an Ion Max source with a HESI probe, both from Thermo Fisher Scientific (Bremen, Germany). Instrument settings were as follows: source heater temperature of 100 °C, spray voltage of 3.5 kV, sheath gas flow of 10 arbitrary units, auxiliary gas flow of 5 arbitrary units, capillary temperature of 300 °C, S-lens RF level of 60.0. Each scan cycle consisted of a full scan at a scan range of *m/z* 350–2000 with an AGC target of 1e6, a maximum injection time of 150 ms and a resolution setting of 70,000, followed by 5 data-dependent HCD scans at 28 NCE (corresponding to 27.5 eV for the selected peptide) with an AGC target of 5e5, a maximum injection time of 150 ms and a resolution setting of 17,500. Both instruments were mass calibrated using Pierce LTQ Velos ESI Positive Ion Calibration Solution from Life Technologies (Vienna, Austria) and AHFP.

Data evaluation

Isotopically resolved mass spectra were deconvoluted using the Xtract algorithm implemented in the Xcalibur software version 3.0.63 (Thermo Fisher Scientific, Waltham, MA, USA). Annotation of glycoforms and other PTMs was conducted using MoFi v1.0[54]. Fc/2 amino acid sequences were derived from constant heavy chain entries in the Uniprot database (Supplementary Fig. S-2). MoFi-assisted peak assignment was based on monoisotopic masses with a mass tolerance of ± 50 ppm assuming intrachain disulphide bridges to be intact and interchain disulphide bonds to be reduced (see amino acid sequences Supplementary Fig. S-2). A library containing common *N*-glycan structures as determined by glycopeptide analysis[38] of murine IgGs was used (Supplementary Table S-2). For relative quantification of Fc/2 *N*-glycoforms, XICCs were generated and evaluated using the Chromeleon Chromatography Data System, version 7.2 SR3 (Thermo Fisher Scientific, Waltham, MA, USA), as previously described[11]: XICC ranges were determined based on a simulated isotopic distribution for the atomic composition of Fc/2 plus the respective glycan taking into account the ten most abundant isotope peaks. Spectra were simulated using the Xcalibur software. XICCs were then generated for charge states 10 + to 15 + for relative quantification of subclasses and Fc/2 glycoforms based on integrated peak areas of these XICCs. Fc/2 masses were calculated using the software tool GPMAW 9.51 rel. 0314 (Lighthouse Data, Odense, Denmark)[67]. AIF data were evaluated using the software ProSight Lite v1.4 Build 1.4.6 provided by the Kelleher Research Group (Northwestern University, Evanston, IL, USA)[68]; mass tolerance for annotation of b- and y-fragments was set to 25 ppm. For statistical evaluation and plotting of data we used GraphPad Prism version 5.01. Principal component analysis was performed with Simca 13.0.3 (Umetrics, Sartorius Stedim Biotech, Göttingen, Germany) using unit variances and mean centering for data pre-processing.

Data availability

The mass spectrometry proteomics data have been deposited to the ProteomeXchange Consortium via the PRIDE partner repository with the dataset identifier PXD014710[69].

Received: 9 December 2019; Accepted: 9 October 2020
Published online: 22 October 2020

References

1. Lermyte, F., Tsybin, Y. O., O'Connor, P. B. & Loo, J. A. Top or middle? Up or down? Toward a standard lexicon for protein top-down and allied mass spectrometry approaches. *J. Am. Soc. Mass Spectrom.* **30**, 1149–1157. https://doi.org/10.1007/s13361-019-02201-x (2019).
2. Regl, C. *et al.* Dilute-and-shoot analysis of therapeutic monoclonal antibody variants in fermentation broth: a method capability study. *MAbs* **11**, 569–582. https://doi.org/10.1080/19420862.2018.1563034 (2019).
3. Rosati, S. *et al.* In-depth qualitative and quantitative analysis of composite glycosylation profiles and other micro-heterogeneity on intact monoclonal antibodies by high-resolution native mass spectrometry using a modified Orbitrap. *MAbs* **5**, 917–924. https://doi.org/10.4161/mabs.26282 (2013).
4. Beck, A., Wagner-Rousset, E., Ayoub, D., Van Dorsselaer, A. & Sanglier-Cianferani, S. Characterization of therapeutic antibodies and related products. *Anal. Chem.* **85**, 715–736. https://doi.org/10.1021/ac3032355 (2013).
5. Yang, Y., Wang, G., Song, T., Lebrilla, C. B. & Heck, A. J. R. Resolving the micro-heterogeneity and structural integrity of monoclonal antibodies by hybrid mass spectrometric approaches. *MAbs* **9**, 638–645. https://doi.org/10.1080/19420862.2017.1290033 (2017).
6. Thompson, N. J., Rosati, S., Rose, R. J. & Heck, A. J. The impact of mass spectrometry on the study of intact antibodies: from post-translational modifications to structural analysis. *Chem. Commun.* **49**, 538–548. https://doi.org/10.1039/c2cc36755f (2013).
7. Fussl, F. *et al.* Comprehensive characterisation of the heterogeneity of adalimumab via charge variant analysis hyphenated on-line to native high resolution Orbitrap mass spectrometry. *MAbs* **11**, 116–128. https://doi.org/10.1080/19420862.2018.1531664 (2019).
8. Wohlschlager, T. *et al.* Native mass spectrometry combined with enzymatic dissection unravels glycoform heterogeneity of biopharmaceuticals. *Nat. Commun.* **9**, 1713. https://doi.org/10.1038/s41467-018-04061-7 (2018).
9. Fekete, S., Guillarme, D., Sandra, P. & Sandra, K. Chromatographic, electrophoretic, and mass spectrometric methods for the analytical characterization of protein biopharmaceuticals. *Anal. Chem.* **88**, 480–507. https://doi.org/10.1021/acs.analchem.5b04561 (2016).
10. D'Atri, V., Fekete, S., Beck, A., Lauber, M. & Guillarme, D. Hydrophilic interaction chromatography hyphenated with mass spectrometry: a powerful analytical tool for the comparison of originator and biosimilar therapeutic monoclonal antibodies at the middle-up level of analysis. *Anal. Chem.* **89**, 2086–2092. https://doi.org/10.1021/acs.analchem.6b04726 (2017).
11. Regl, C., Wohlschlager, T., Holzmann, J. & Huber, C. G. A generic HPLC method for absolute quantification of oxidation in monoclonal antibodies and Fc-fusion proteins using UV and MS detection. *Anal. Chem.* **89**, 8391–8398. https://doi.org/10.1021/acs.analchem.7b01755 (2017).
12. Sjogren, J., Olsson, F. & Beck, A. Rapid and improved characterization of therapeutic antibodies and antibody related products using IdeS digestion and subunit analysis. *Analyst* **141**, 3114–3125. https://doi.org/10.1039/c6an00071a (2016).
13. Chevreux, G., Tilly, N. & Bihoreau, N. Fast analysis of recombinant monoclonal antibodies using IdeS proteolytic digestion and electrospray mass spectrometry. *Anal. Biochem.* **415**, 212–214 (2011).
14. Nimmerjahn, F. & Ravetch, J. V. Fcgamma receptors: old friends and new family members. *Immunity* **24**, 19–28. https://doi.org/10.1016/j.immuni.2005.11.010 (2006).

15. Vidarsson, G., Dekkers, G. & Rispens, T. IgG subclasses and allotypes: from structure to effector functions. *Front. Immunol.* **5**, 520 (2014).
16. Dekkers, G. *et al.* Affinity of human IgG subclasses to mouse Fc gamma receptors. *MAbs* **9**, 767–773. https://doi.org/10.1080/19420862.2017.1323159 (2017).
17. Nimmerjahn, F. & Ravetch, J. V. Divergent immunoglobulin g subclass activity through selective Fc receptor binding. *Science* **310**, 1510–1512. https://doi.org/10.1126/science.1118948 (2005).
18. Kao, D. *et al.* A monosaccharide residue is sufficient to maintain mouse and human IgG subclass activity and directs IgG effector functions to cellular Fc receptors. *Cell Rep.* **13**, 2376–2385. https://doi.org/10.1016/j.celrep.2015.11.027 (2015).
19. Arnold, J. N., Wormald, M. R., Sim, R. B., Rudd, P. M. & Dwek, R. A. The impact of glycosylation on the biological function and structure of human immunoglobulins. *Annu. Rev. Immunol.* **25**, 21–50. https://doi.org/10.1146/annurev.immunol.25.022106.141702 (2007).
20. Feige, M. J. *et al.* Structure of the murine unglycosylated IgG1 Fc fragment. *J. Mol. Biol.* **391**, 599–608 (2009).
21. Krapp, S., Mimura, Y., Jefferis, R., Huber, R. & Sondermann, P. Structural analysis of human IgG-Fc glycoforms reveals a correlation between glycosylation and structural integrity. *J. Mol. Biol.* **325**, 979–989. https://doi.org/10.1016/s0022-2836(02)01250-0 (2003).
22. Tradtrantip, L., Ratelade, J., Zhang, H. & Verkman, A. S. Enzymatic deglycosylation converts pathogenic neuromyelitis optica anti-aquaporin-4 immunoglobulin G into therapeutic antibody. *Ann. Neurol.* **73**, 77–85. https://doi.org/10.1002/ana.23741 (2013).
23. Kronimus, Y., Dodel, R., Galuska, S. P. & Neumann, S. IgG Fc N-glycosylation: alterations in neurologic diseases and potential therapeutic target?. *J. Autoimmun.* **96**, 14–23. https://doi.org/10.1016/j.jaut.2018.10.006 (2018).
24. Banda, N. K. *et al.* Initiation of the alternative pathway of murine complement by immune complexes is dependent on N-glycans in IgG antibodies. *Arthritis Rheum.* **58**, 3081–3089. https://doi.org/10.1002/art.23865 (2008).
25. Maverakis, E. *et al.* Glycans in the immune system and the altered glycan theory of autoimmunity: a critical review. *J. Autoimmun.* **57**, 1–13. https://doi.org/10.1016/j.jaut.2014.12.002 (2015).
26. Chen, G. *et al.* Human IgG Fc-glycosylation profiling reveals associations with age, sex, female sex hormones and thyroid cancer. *J. Proteomics* **75**, 2824–2834. https://doi.org/10.1016/j.jprot.2012.02.001 (2012).
27. Parekh, R., Roitt, I., Isenberg, D., Dwek, R. & Rademacher, T. Age-related galactosylation of the N-linked oligosaccharides of human serum IgG. *J. Exp. Med.* **167**, 1731–1736. https://doi.org/10.1084/jem.167.5.1731 (1988).
28. Kristic, J. *et al.* Profiling and genetic control of the murine immunoglobulin G glycome. *Nat. Chem. Biol.* **14**, 516–524. https://doi.org/10.1038/s41589-018-0034-3 (2018).
29. Gudelj, I., Lauc, G. & Pezer, M. Immunoglobulin G glycosylation in aging and diseases. *Cell. Immunol.* **333**, 65–79. https://doi.org/10.1016/j.cellimm.2018.07.009 (2018).
30. Eckl-Dorna, J. *et al.* Allergen-specific antibodies regulate secondary allergen-specific immune responses. *Front. Immunol.* **9**, 3131. https://doi.org/10.3389/fimmu.2018.03131 (2018).
31. Epp, A. *et al.* Sialylation of IgG antibodies inhibits IgG-mediated allergic reactions. *J. Allergy Clin. Immunol.* **141**, 399–402. https://doi.org/10.1016/j.jaci.2017.06.021 (2018).
32. Wuhrer, M. *et al.* Glycosylation profiling of immunoglobulin G (IgG) subclasses from human serum. *Proteomics* **7**, 4070–4081. https://doi.org/10.1002/pmic.200700289 (2007).
33. Mahan, A. E. *et al.* Antigen-specific antibody glycosylation is regulated via vaccination. *PLoS Pathog.* **12**, e1005456. https://doi.org/10.1371/journal.ppat.1005456 (2016).
34. Schwab, I. & Nimmerjahn, F. Intravenous immunoglobulin therapy: how does IgG modulate the immune system?. *Nat. Rev. Immunol.* **13**, 176–189. https://doi.org/10.1038/nri3401 (2013).
35. Falck, D., Jansen, B. C., de Haan, N. & Wuhrer, M. High-throughput analysis of IgG Fc glycopeptides by LC-MS. *Methods Mol. Biol.* **1503**, 31–47. https://doi.org/10.1007/978-1-4939-6493-2_4 (2017).
36. Klein-Schneegans, A. S., Gaveriaux, C., Fonteneau, P. & Loor, F. Indirect double sandwich ELISA for the specific and quantitative measurement of mouse IgM, IgA and IgG subclasses. *J. Immunol. Methods* **119**, 117–125. https://doi.org/10.1016/0022-1759(89)90388-8 (1989).
37. Zaytseva, O. O. *et al.* MIgGGly (mouse IgG glycosylation analysis) - a high-throughput method for studying Fc-linked IgG N-glycosylation in mice with nanoUPLC-ESI-MS. *Sci. Rep.* **8**, 13688. https://doi.org/10.1038/s41598-018-31844-1 (2018).
38. de Haan, N. *et al.* The N-glycosylation of mouse immunoglobulin G (IgG)-fragment crystallizable differs between IgG subclasses and strains. *Front. Immunol.* **8**, 608. https://doi.org/10.3389/fimmu.2017.00608 (2017).
39. Maresch, D. & Altmann, F. Isotype-specific glycosylation analysis of mouse IgG by LC-MS. *Proteomics* **16**, 1321–1330. https://doi.org/10.1002/pmic.201500367 (2016).
40. Selman, M. H. *et al.* Fc specific IgG glycosylation profiling by robust nano-reverse phase HPLC-MS using a sheath-flow ESI sprayer interface. *J. Proteomics* **75**, 1318–1329. https://doi.org/10.1016/j.jprot.2011.11.003 (2012).
41. Goetze, A. M., Zhang, Z., Liu, L., Jacobsen, F. W. & Flynn, G. C. Rapid LC-MS screening for IgG Fc modifications and allelic variants in blood. *Mol. Immunol.* **49**, 338–352. https://doi.org/10.1016/j.molimm.2011.09.002 (2011).
42. Leblanc, Y., Romanin, M., Bihoreau, N. & Chevreux, G. LC-MS analysis of polyclonal IgGs using IdeS enzymatic proteolysis for oxidation monitoring. *J. Chromatogr. B Analyt. Technol. Biomed. Life Sci.* **961**, 1–4. https://doi.org/10.1016/j.jchromb.2014.04.053 (2014).
43. Collin, M. & Olsén, A. Effect of SpeB and EndoS from *Streptococcus pyogenes* on human immunoglobulins. *Infect. Immun.* **69**, 7187–7189. https://doi.org/10.1128/iai.69.11.7187-7189.2001 (2001).
44. Vrtala, S. *et al.* Molecular, immunological, and structural characterization of Phl p 6, a major allergen and P-particle-associated protein from Timothy grass (*Phleum pratense*) pollen. *J. Immunol.* **163**, 5489–5496 (1999).
45. Persson, H., Vindebro, R. & von Pawel-Rammingen, U. The streptococcal cysteine protease SpeB is not a natural immunoglobulin-cleaving enzyme. *Infect Immun.* **81**, 2236–2241. https://doi.org/10.1128/IAI.00168-13 (2013).
46. Von Pawel-Rammingen, U. & Bjorck, L. IdeS and SpeB: immunoglobulin-degrading cysteine proteinases of *Streptococcus pyogenes*. *Curr. Opin. Microbiol.* **6**, 50–55. https://doi.org/10.1016/s1369-5274(03)00003-1 (2003).
47. Nelson, D. C., Garbe, J. & Collin, M. Cysteine proteinase SpeB from *Streptococcus pyogenes*: a potent modifier of immunologically important host and bacterial proteins. *Biol. Chem.* **392**, 1077–1088. https://doi.org/10.1515/BC.2011.208 (2011).
48. Adetugbo, K. Evolution of immunoglobulin subclasses. Primary structure of a murine myeloma gamma1 chain. *J. Biol. Chem.* **253**, 6068–6075 (1978).
49. Bankert, B. & Mazzaferro, P. *Biochemistry of Immunoglobulins. The Clinical Chemistry of Laboratory Animals* 231–265 (Pergamon Press, New York, 1999).
50. Abdelmoula, M. *et al.* IgG3 is the major source of cryoglobulins in mice. *J. Immunol.* **143**, 526–532 (1989).
51. Hsieh, C. S., Macatonia, S. E., O'Garra, A. & Murphy, K. M. T cell genetic background determines default T helper phenotype development in vitro. *J. Exp. Med.* **181**, 713–721. https://doi.org/10.1084/jem.181.2.713 (1995).
52. Hage, D. S. & Cazes, J. *Handbook of affinity chromatography* 2nd edn, 377–381 (CRC Press, Boca Raton, 2005).
53. Ferreira, D. M., Darrieux, M., Oliveira, M. L., Leite, L. C. & Miyaji, E. N. Optimized immune response elicited by a DNA vaccine expressing pneumococcal surface protein a is characterized by a balanced immunoglobulin G1 (IgG1)/IgG2a ratio and proinflammatory cytokine production. *Clin. Vaccine Immunol.* **15**, 499–505. https://doi.org/10.1128/CVI.00400-07 (2008).

54. Skala, W., Wohlschlager, T., Senn, S., Huber, G. E. & Huber, C. G. MoFi: a software tool for annotating glycoprotein mass spectra by integrating hybrid data from the intact protein and glycopeptide level. *Anal. Chem.* **90**, 5728–5736. https://doi.org/10.1021/acs.analchem.8b00019 (2018).
55. Ruhaak, L. R., Xu, G., Li, Q., Goonatilleke, E. & Lebrilla, C. B. Mass spectrometry approaches to glycomic and glycoproteomic analyses. *Chem. Rev.* **118**, 7886–7930. https://doi.org/10.1021/acs.chemrev.7b00732 (2018).
56. Kao, D. *et al.* IgG subclass and vaccination stimulus determine changes in antigen specific antibody glycosylation in mice. *Eur. J. Immunol.* **47**, 2070–2079. https://doi.org/10.1002/eji.201747208 (2017).
57. Gahoual, R. *et al.* Detailed characterization of monoclonal antibody receptor interaction using affinity liquid chromatography hyphenated to native mass spectrometry. *Anal. Chem.* **89**, 5404–5412. https://doi.org/10.1021/acs.analchem.7b00211 (2017).
58. Zhang, Z., Goldschmidt, T. & Salter, H. Possible allelic structure of IgG2a and IgG2c in mice. *Mol. Immunol.* **50**, 169–171. https://doi.org/10.1016/j.molimm.2011.11.006 (2012).
59. Sanchez Acosta, G. *et al.* IgE-blocking antibodies following SLIT with recombinant Mal d 1 accord with improved apple allergy. *J. Allergy Clin. Immunol.* https://doi.org/10.1016/j.jaci.2020.03.015 (2020).
60. Jegerlehner, A. *et al.* TLR9 signaling in B cells determines class switch recombination to IgG2a. *J. Immunol.* **178**, 2415–2420. https://doi.org/10.4049/jimmunol.178.4.2415 (2007).
61. van Aalst, S., Ludwig, I. S., van der Zee, R., van Eden, W. & Broere, F. Bystander activation of irrelevant CD4+ T cells following antigen-specific vaccination occurs in the presence and absence of adjuvant. *PLoS ONE* **12**, e0177365. https://doi.org/10.1371/journal.pone.0177365 (2017).
62. Selman, M. H. *et al.* Changes in antigen-specific IgG1 Fc N-glycosylation upon influenza and tetanus vaccination. *Mol. Cell Proteomics* **11**, 014563. https://doi.org/10.1074/mcp.M111.014563 (2012).
63. Williams, J. W., Tjota, M. Y. & Sperling, A. I. The contribution of allergen-specific IgG to the development of th2-mediated airway inflammation. *J Allergy* **2012**, 236075. https://doi.org/10.1155/2012/236075 (2012).
64. van Blokland, S. C. & Versnel, M. A. Pathogenesis of Sjogren's syndrome: characteristics of different mouse models for autoimmune exocrinopathy. *Clin. Immunol.* **103**, 111–124. https://doi.org/10.1006/clim.2002.5189 (2002).
65. Asquith, D. L., Miller, A. M., McInnes, I. B. & Liew, F. Y. Animal models of rheumatoid arthritis. *Eur. J. Immunol.* **39**, 2040–2044. https://doi.org/10.1002/eji.200939578 (2009).
66. Natsuume-Sakai, S., Motonishi, K. & Migita, S. Quantitative estimations of five classes of immunoglobulin in inbred mouse strains. *Immunology* **32**, 861–866 (1977).
67. Peri, S., Steen, H. & Pandey, A. GPMAW: a software tool for analyzing proteins and peptides. *Trends Biochem. Sci.* **26**, 687–689. https://doi.org/10.1016/s0968-0004(01)01954-5 (2001).
68. Fellers, R. T. *et al.* ProSight Lite: graphical software to analyze top-down mass spectrometry data. *Proteomics* **15**, 1235–1238. https://doi.org/10.1002/pmic.201570050 (2015).
69. Perez-Riverol, Y. *et al.* The PRIDE database and related tools and resources in 2019: improving support for quantification data. *Nucleic Acids Res.* **47**, D442–D450. https://doi.org/10.1093/nar/gky1106 (2019).

Acknowledgements

The financial support by the Austrian Federal Ministry for Digital and Economic Affairs, the National Foundation for Research, Technology and Development, the Christian Doppler Research Association as well as a Start-up Grant of the State of Salzburg is gratefully acknowledged. C. B. acknowledges a research stipend form the István and Agnes Halász Foundation, Saarbrücken, Germany. This work was supported by a grant from the Austrian Science Fund (FWF, W1213). We thank Peter Hammerl and Angelika Stöcklinger (Department of Biosciences, University of Salzburg) for animal handling and scientific discussions and Wolfgang Esser-Skala (Department of Biosciences, University of Salzburg) for scientific discussions. We are grateful to Genovis AB (Lund, Sweden) for providing the SpeB protease.

Author contributions

C.B., C.R., C.G.H., R.W., and T.W. conceived the study. C.B., C.R., and P.W. performed the experiments; C.B., R.W., and T.W. analysed and interpreted the data. C.B., C.G.H., and T.W. drafted the manuscript. All authors reviewed the manuscript.

Funding

The salary of Therese Wohlschlager is fully funded; Christian G. Huber's salary is partly funded by the Christian Doppler Laboratory for Innovative Tools for Biosimilar Characterization which receives financial support from Novartis and Thermo Fisher Scientific.

Competing interests

The authors declare no competing interests.

Additional information

Supplementary information is available for this paper at https://doi.org/10.1038/s41598-020-75045-1.

Correspondence and requests for materials should be addressed to T.W.

Reprints and permissions information is available at www.nature.com/reprints.

Publisher's note Springer Nature remains neutral with regard to jurisdictional claims in published maps and institutional affiliations.

Open Access This article is licensed under a Creative Commons Attribution 4.0 International License, which permits use, sharing, adaptation, distribution and reproduction in any medium or format, as long as you give appropriate credit to the original author(s) and the source, provide a link to the Creative Commons licence, and indicate if changes were made. The images or other third party material in this article are included in the article's Creative Commons licence, unless indicated otherwise in a credit line to the material. If material is not included in the article's Creative Commons licence and your intended use is not permitted by statutory regulation or exceeds the permitted use, you will need to obtain permission directly from the copyright holder. To view a copy of this licence, visit http://creativecommons.org/licenses/by/4.0/.

© The Author(s) 2020

SUPPLEMENTARY INFORMATION

Towards middle-up analysis of polyclonal antibodies: subclass-specific *N*-glycosylation profiling of murine immunoglobulin G (IgG) by means of HPLC-MS

Constantin Blöchl[1], Christof Regl[1,2], Christian G. Huber[1,2], Petra Winter[3], Richard Weiss[3], and Therese Wohlschlager[1,2,*]

[1]Department of Biosciences, Bioanalytical Research Labs, University of Salzburg, Hellbrunner Straße 34, 5020 Salzburg, Austria

[2]Christian Doppler Laboratory for Innovative Tools for Biosimilar Characterization, University of Salzburg, Hellbrunner Straße 34, 5020 Salzburg, Austria

[3]Department of Biosciences, Division of Allergy and Immunology, University of Salzburg, Hellbrunner Straße 34, 5020 Salzburg, Austria

*Correspondence should be addressed to therese.wohlschlager@sbg.ac.at

Table of contents

Figure S-1: Schematic workflow for SpeB cleavage site determination in HC portions Page S-2

Figure S-2: Amino acid sequences of HC constant regions of murine IgG subclasses Page S-3

Figure S-3: Fragment ion spectrum of tryptic peptide [269-286] of IgG1 from BALB/c Page S-4

Figure S-4: Separation and quantification of main and minor Fc/2 cleavage products Page S-5

Figure S-5: Fractional subclass abundances of total IgGs from BALB/c and C57BL/6 Page S-6

Figure S-6: Raw mass spectra of IgG1, IgG2a and IgG2b from BALB/c Page S-7

Figure S-7: Identification of oxidised tryptic peptide [179-194] of IgG1 from BALB/c Page S-8

Figure S-8: Deconvoluted mass spectra of Fc/2 from monoclonal IgG1 and IgG2b Page S-9

Figure S-9: Schematic workflow for Phl p 6 vaccination study Page S-10

Figure S-10: IgG subclass abundances after Phl p 6 vaccination Page S-11

Figure S-11: Subclass-specific glycosylation profiles of total IgG after Phl p 6 vaccination Page S-12

Figure S-12: Glycoform abundances of IgG1 from mouse individuals Page S-13

Table S-1: SpeB cleavage products of murine IgG subclasses Page S-14

Table S-2: *N*-glycan structures considered in glycoform assignment Page S-15

SI References Page S-18

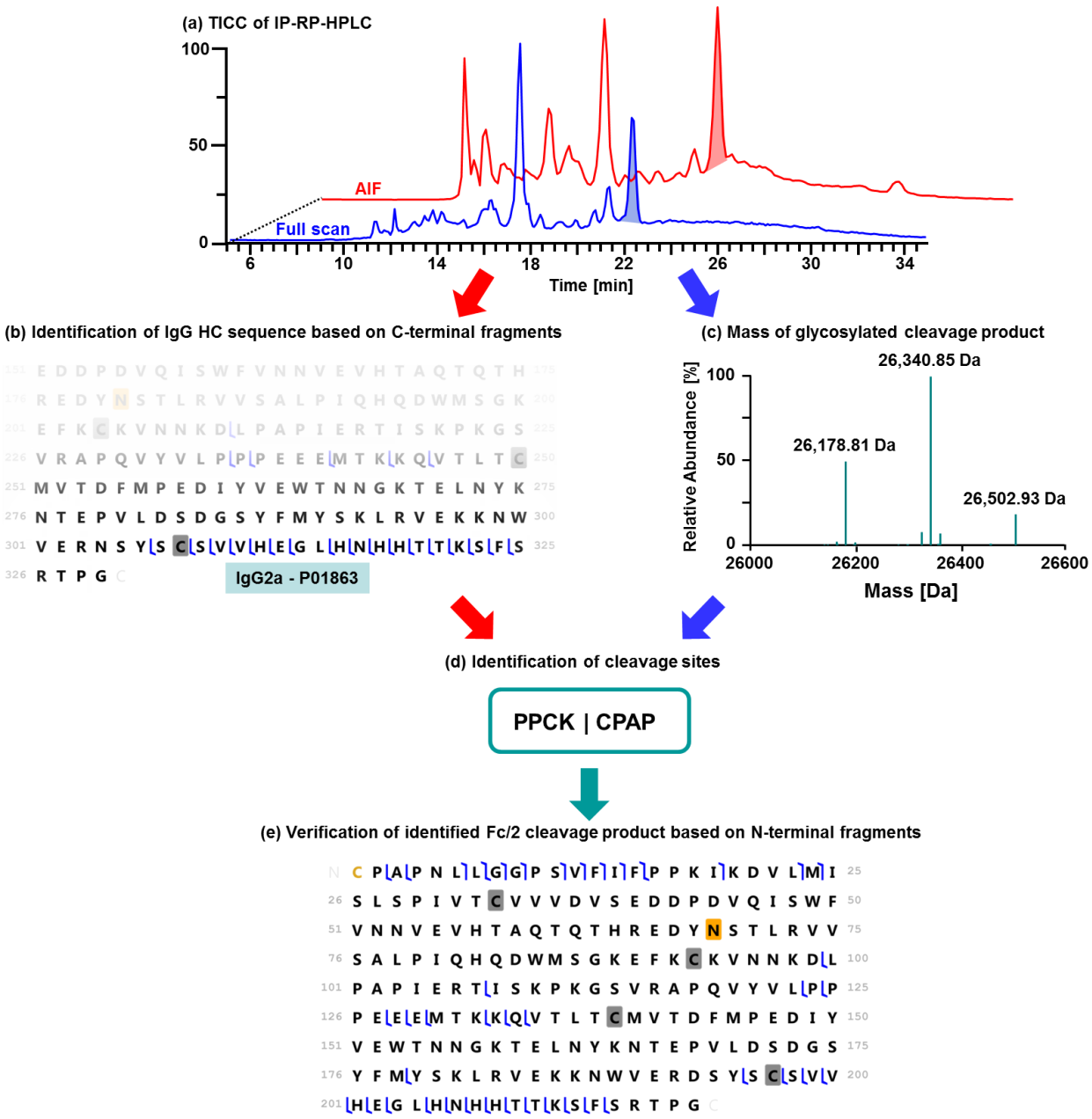

Figure S-1. Schematic workflow for SpeB cleavage site determination in HC portions of IgG as shown for polyclonal IgG2a (P01863) from BALB/c. (a) SpeB cleavage products are separated by IP-RP-HPLC and detected in full MS/AIF mode. The AIF trace is depicted at a time offset of 4.0 min. (b) Fragment spectra obtained by AIF are deconvoluted and searched against the sequences provided in Fig. S-2 using the ProSight software.[1] The constant HC sequence is identified based on the assigned y-ions, i.e. C-terminal fragments (blue marks). (c) Masses of the glycosylated cleavage product are derived from the corresponding full scan spectra. (d) The cleavage site is determined based on the mass of the obtained proteolytic product taking into account the G1F glycoform. The process is supported by the GPMAW software.[2] (e) For further confirmation, the sequence of the identified proteolytic product is searched against AIF spectra to match b-ions, i.e. N-terminal fragments, using the ProSight software. Fragmentation data for all identified cleavage sites are available as Supplementary Excel file.

IgG1 (P01868)

```
1       AKTTPPSVYP LAPGSAAQTN SMVTLGCLVK GYFPEPVTVT WNSGSLSSGV HTFPAVLQSD
61      LYTLSSSVTV PSSPRPSETV TCNVAHPASS TKVDKKIVPR DCGCKPCICT VPEVSSVFIF
121     PPKPKDVLTI TLTPKVTCVV VDISKDDPEV QFSWFVDDVE VHTAQTQPRE EQFNSTFRSV
181     SELPIMHQDW LNGKEFKCRV NSAAFPAPIE KTISKTKGRP KAPQVYTIPP PKEQMAKDKV
241     SLTCMITDFF PEDITVEWQW NGQPAENYKN TQPIMDTDGS YFVYSKLNVQ KSNWEAGNTF
301     TCSVLHEGLH NHHTEKSLSH SPGK
```

IgG1i (A0A075B5P4)

```
1       XKTTPPSVYP LAPGSAAQTN SMVTLGCLVK GYFPEPVTVT WNSGSLSSGV HTFPAVLQSD
61      LYTLSSSVTV PSSTWPSQTV TCNVAHPASS TKVDKKIVPR DCGCKPCICT VPEVSSVFIF
121     PPKPKDVLTI TLTPKVTCVV VDISKDDPEV QFSWFVDDVE VHTAQTKPRE EQINSTFRSV
181     SELPIMHQDW LNGKEFKCRV NSAAFPAPIE KTISKTKGRP KAPQVYTIPP PKEQMAKDKV
241     SLTCMITNFF PEDITVEWQW NGQPAENYKN TQPIMDTDGS YFVYSKLNVQ KSNWEAGNTF
301     TCSVLHEGLH NHHTEKSLSH SPGK
```

IgG2a (P01863)

```
1       AKTTAPSVYP LAPVCGDTTG SSVTLGCLVK GYFPEPVTLT WNSGSLSSGV HTFPAVLQSD
61      LYTLSSSVTV TSSTWPSQSI TCNVAHPASS TKVDKKIEPR GPTIKPCPPC KCPAPNLLGG
121     PSVFIFPPKI KDVLMISLSP IVTCVVVDVS EDDPDVQISW FVNNVEVHTA QTQTHREDYN
181     STLRVVSALP IQHQDWMSGK EFKCKVNNKD LPAPIERTIS KPKGSVRAPQ VYVLPPPEEE
241     MTKKQVTLTC MVTDFMPEDI YVEWTNNGKT ELNYKNTEPV LDSDGSYFMY SKLRVEKKNW
301     VERNSYSCSV VHEGLHNHHT TKSFSRTPGK
```

IgG2b (P01867)

```
1       KTTPPSVYPL APGCGDTTGS SVTLGCLVKG YFPESVTVTW NSGSLSSSVH TFPALLQSGL
61      YTMSSSVTVP SSTWPSQTVT CSVAHPASST TVDKKLEPSG PISTINPCPP CKECHKCPAP
121     NLEGGPSVFI FPPNIKDVLM ISLTPKVTCV VVDVSEDDPD VQISWFVNNV EVHTAQTQTH
181     REDYNSTIRV VSTLPIQHQD WMSGKEFKCK VNNKDLPSPI ERTISKIKGL VRAPQVYILP
241     PPAEQLSRKD VSLTCLVVGF NPGDISVEWT SNGHTEENYK DTAPVLDSDG SYFIYSKLNM
301     KTSKWEKTDS FSCNVRHEGL KNYYLKKTIS RSPGK
```

IgG2bi (A0A075B5P3)

```
1       XKTTPPSVYP LAPGCGDTTG SSVTLGCLVK GYFPESVTVT WNSGSLSSSV HTFPALLQSG
61      LYTMSSSVTV PSSTWPSQTV TCSVAHPASS TTVDKKLEPS GPISTINPCP PCKECHKCPA
121     PNLEGGPSVF IFPPNIKDVL MISLTPKVTC VVVDVSEDDP DVRISWFVNN VEVHTAQTQT
181     HREDYNSTIR VVSALPIQHQ DWMSGKEFKC KVNNKDLPSP IERTISKIKG LVRAPQVYIL
241     PPPAEQLSRK DVSLTCLVVG FNPGDISVEW TSNGHTEENY KDTAPVLDSD GSYFIYSKLD
301     IKTSKWEKTD SFSCNVRHEG LKNYYLKKTI SRSPGK
```

IgG2c (A0A0A6YY53)

```
1       XKTTAPSVYP LAPVCGGTTG SSVTLGCLVK GYFPEPVTLT WNSGSLSSGV HTFPALLQSG
61      LYTLSSSVTV TSNTWPSQTI TCNVAHPASS TKVDKKIEPR VPITQNPCPP LKECPPCAAP
121     DLLGGPSVFI FPPKIKDVLM ISLSPMVTCV VVDVSEDDPD VQISWFVNNV EVHTAQTQTH
181     REDYNSTLRV VSALPIQHQD WMSGKEFKCK VNNRALPSPI EKTISKPRGP VRAPQVYVLP
241     PPAEEMTKKE FSLTCMITGF LPAEIAVDWT SNGRTEQNYK NTATVLDSDG SYFMYSKLRV
301     QKSTWERGSL FACSVVHEGL HNHLTTKTIS RSLGK
```

IgG3 (P03987)

```
1       TTTAPSVYPL VPGCSDTSGS SVTLGCLVKG YFPEPVTVKW NYGALSSGVR TVSSVLQSGF
61      YSLSSLVTVP SSTWPSQTVI CNVAHPASKT ELIKRIEPRI PKPSTPPGSS CPPGNILGGP
121     SVFIFPPKPK DALMISLTPK VTCVVVDVSE DDPDVHVSWF VDNKEVHTAW TQPREAQYNS
181     TFRVVSALPI QHQDWMRGKE FKCKVNNKAL PAPIERTISK PKGRAQTPQV YTIPPPREQM
241     SKKKVSLTCL VTNFFSEAIS VEWERNGELE QDYKNTPPIL DSDGTYFLYS KLTVDTDSWL
301     QGEIFTCSVV HEALHNHHTQ KNLSRSPGK
```

Figure S-2. Amino acid sequences of HC constant regions of murine IgG subclasses. Uniprot accession numbers of the secreted isoforms are given in brackets. The main cleavage products obtained upon digestion with SpeB are highlighted in grey; minor cleavage sites are marked with a blue line. *N*-glycosylation sites are highlighted in yellow; the C-terminal lysine residue (underlined) is usually absent in polyclonal IgGs but may be present in mAbs. Cysteine residues of intact intramolecular disulphide bonds identified after SpeB cleavage under reducing conditions are highlighted in light blue. Amino acid exchanges (N to D) identified in IgG1 (P01868) of BALB/c mice are highlighted in green (see fragment spectrum in Fig. S-3).

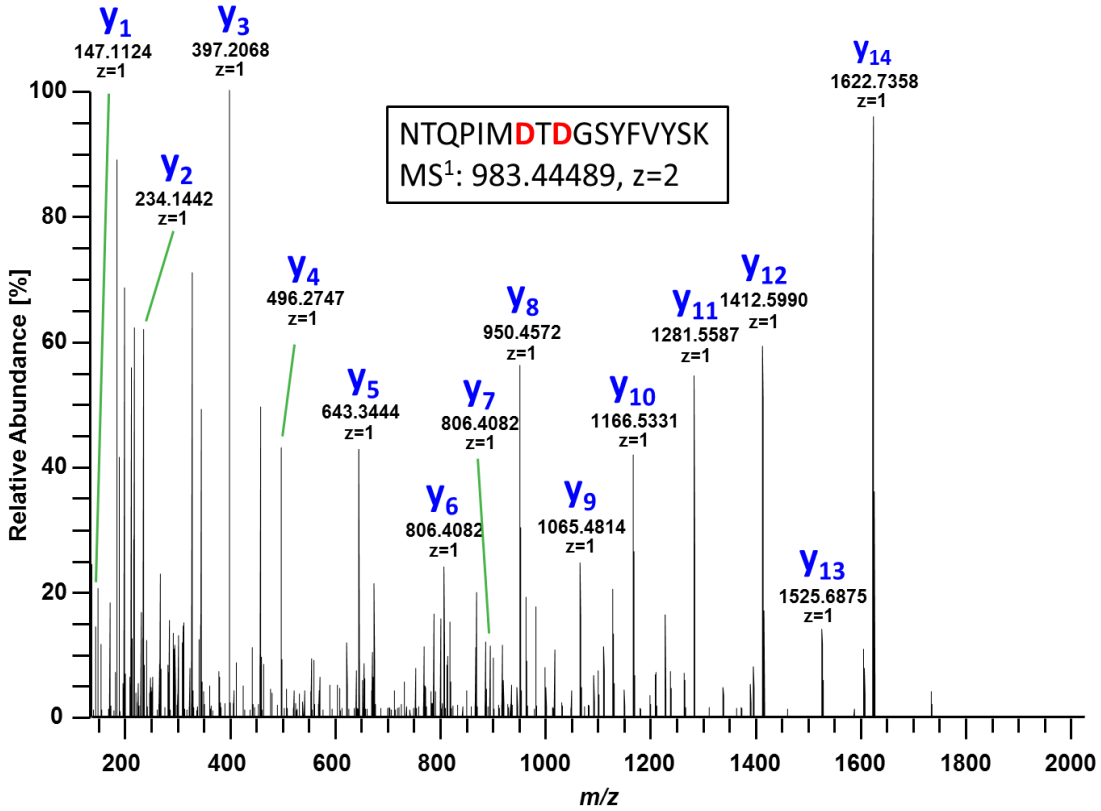

Figure S-3. Fragment ion spectrum of tryptic peptide [269-286] from the constant HC region of IgG1 (P01868, Fig. S-2) from BALB/c. Fragmentation was performed at 27.5 eV in the HCD cell; fragment ions were annotated with the help of GPMAW. Amino acid exchanges (red) are in accordance with a sequence conflict of P01868 listed in the Uniprot database.

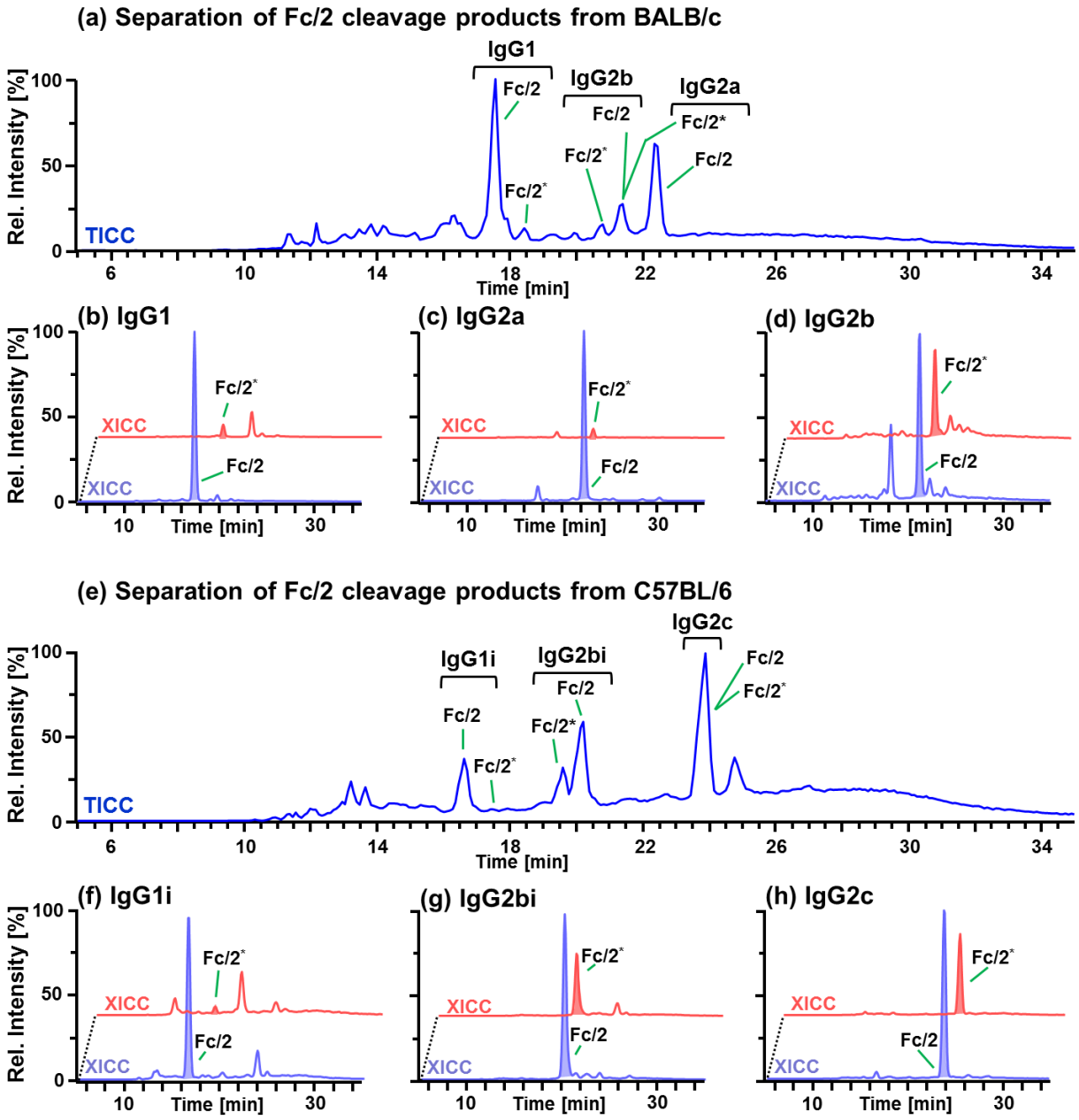

Figure S-4. Separation and quantification of Fc/2 cleavage products generated by SpeB. Main and minor cleavage products are designated Fc/2 and Fc/2*, respectively. (a) TICC of SpeB cleavage products of polyclonal IgGs from BALB/c. XICCs generated for Fc/2 and Fc/2* of (b) IgG1, (c) IgG2a and (d) IgG2b. (e) TICC of SpeB cleavage products of polyclonal IgGs from C57BL/6. XICCs generated for Fc/2 and Fc/2* of (f) IgG1i, (g) IgG2bi and (h) IgG2c. All XICCs were generated for G1F *N*-glycoforms lacking the C-terminal lysine residue; intramolecular disulphide bonds were considered to be intact. Peak areas used for relative quantification are indicated. Relative abundances of main and minor cleavage products are listed in Table S-2. XICCs for Fc/2* are depicted at a time offset of 2.0 min. Note that Fc/2 and Fc/2* cleavage products of each IgG subclass are chromatographically separated with the exception of IgG2c.

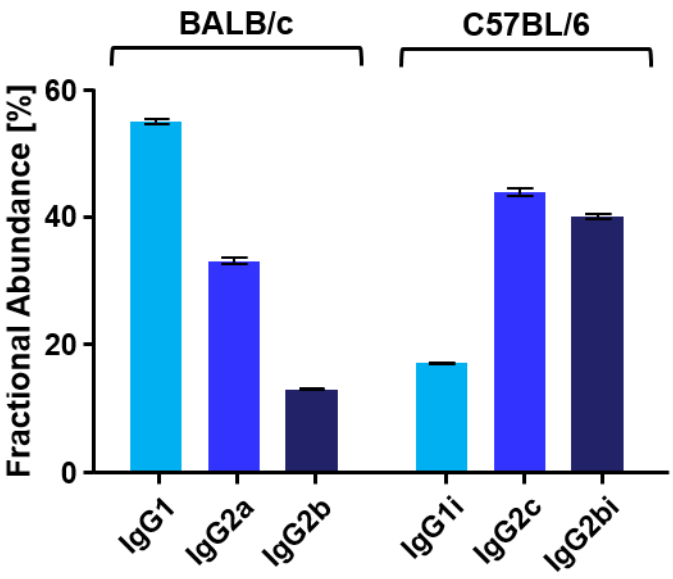

Figure S-5. Fractional subclass abundances of total IgGs from BALB/c and C57BL/6 mouse individuals. Relative abundances were obtained from XICCs of Fc/2 subunits including all detected glycoforms (Supplementary Excel file). Mean values are based on three technical replicates; error bars indicate standard deviations.

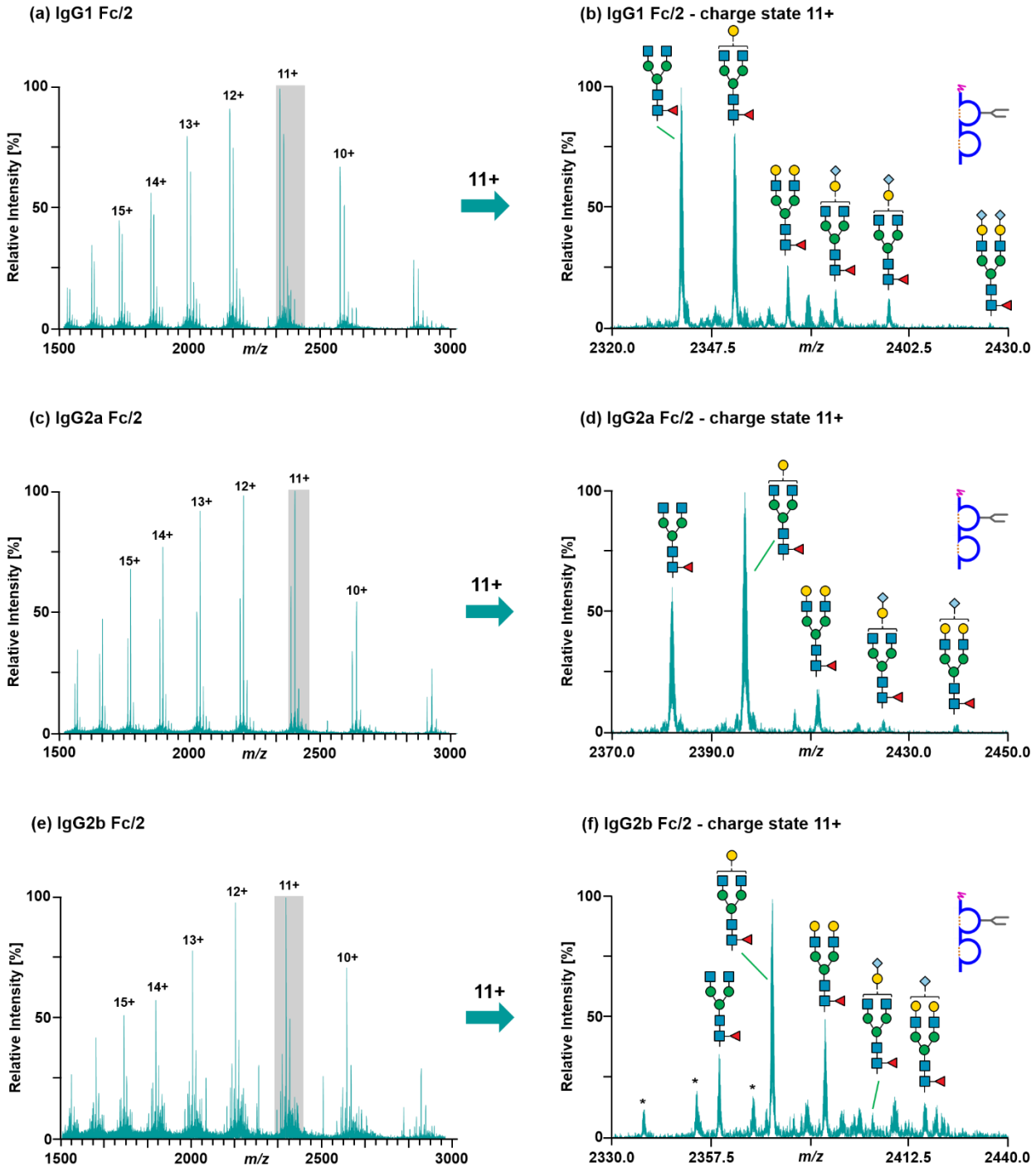

Figure S-6. Exemplary raw mass spectra of Fc/2 from (a) IgG1, (c) IgG2a and (e) IgG2b acquired in a total IgG preparation from a naive BALB/c mouse individual. Charge states used for generation of XICCs are indicated. Zooms of the most abundant charge states with assigned *N*-glycoforms are shown (b, d, f). Asterisks in (f) indicate masses assigned to co-eluting Fc/2* from IgG2a (Fig. S-4a). Note that the signal annotated with G2F may partially arise from the isobaric αG2F structure comprising α-gal.

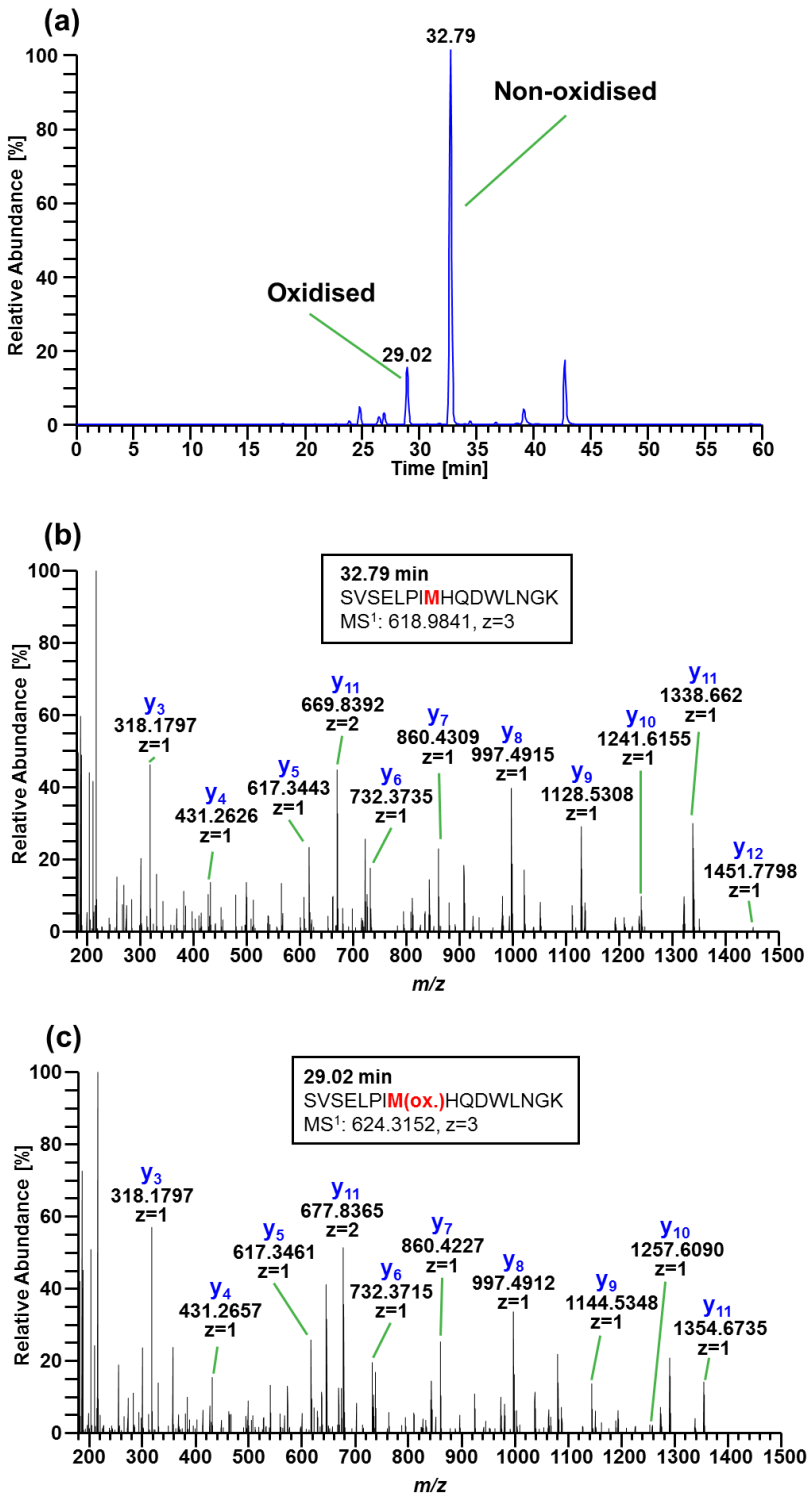

Figure S-7. Identification of oxidised tryptic peptide [179-194] from the constant HC region of IgG1 (P01868, Fig. S-2) from BALB/c. (a) XICC of non-oxidised and oxidised version of tryptic peptide [179-194]. The XICC was generated using the Xcalibur™ software taking into account doubly and triply charged ion species (non-oxidised: 618.6453 *m/z* and 927.4644 *m/z*; oxidised: 623.9770 *m/z* and 935.4618 *m/z;* isolation window ± 0.5 *m/z*). (b) Annotated fragment ion spectrum of the non-oxidised variant. (c) Annotated fragment ion spectrum of the oxidised variant. Fragmentation was performed at 27.5 eV in the HCD cell; fragment ions were annotated with the help of GPMAW.

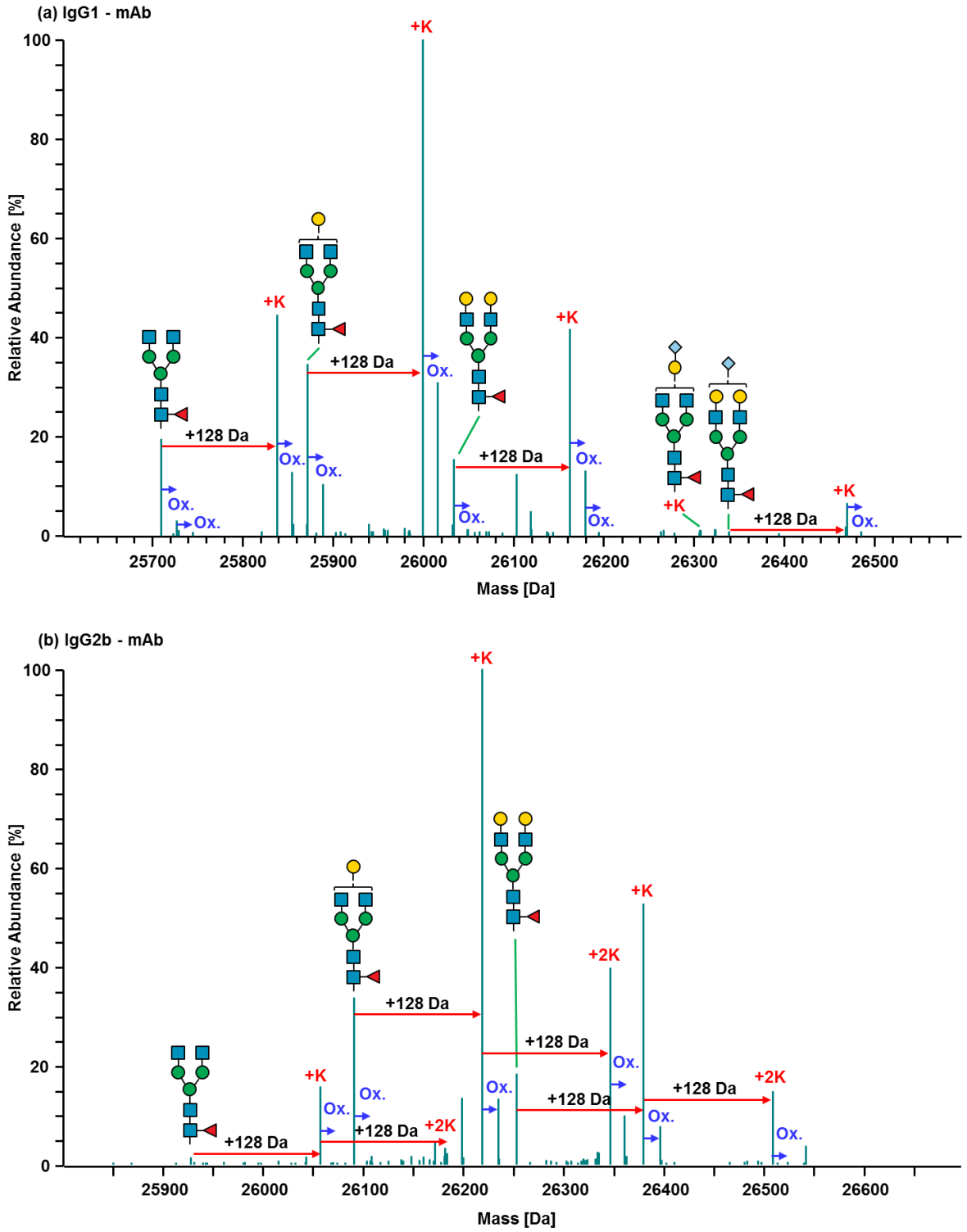

Figure S-8. Deconvoluted mass spectra of Fc/2 derived from (a) monoclonal murine IgG1 (P01868) and (b) monoclonal murine IgG2b (P01867). In addition to the main *N*-glycoforms, variants arising from oxidation (Ox.) or comprising additional lysine residues (+K, +2K) were identified based on characteristic mass shifts (+16 Da and +128 Da, respectively). Note that the signal annotated with G2F may partially arise from the isobaric αG2F structure comprising α-gal.

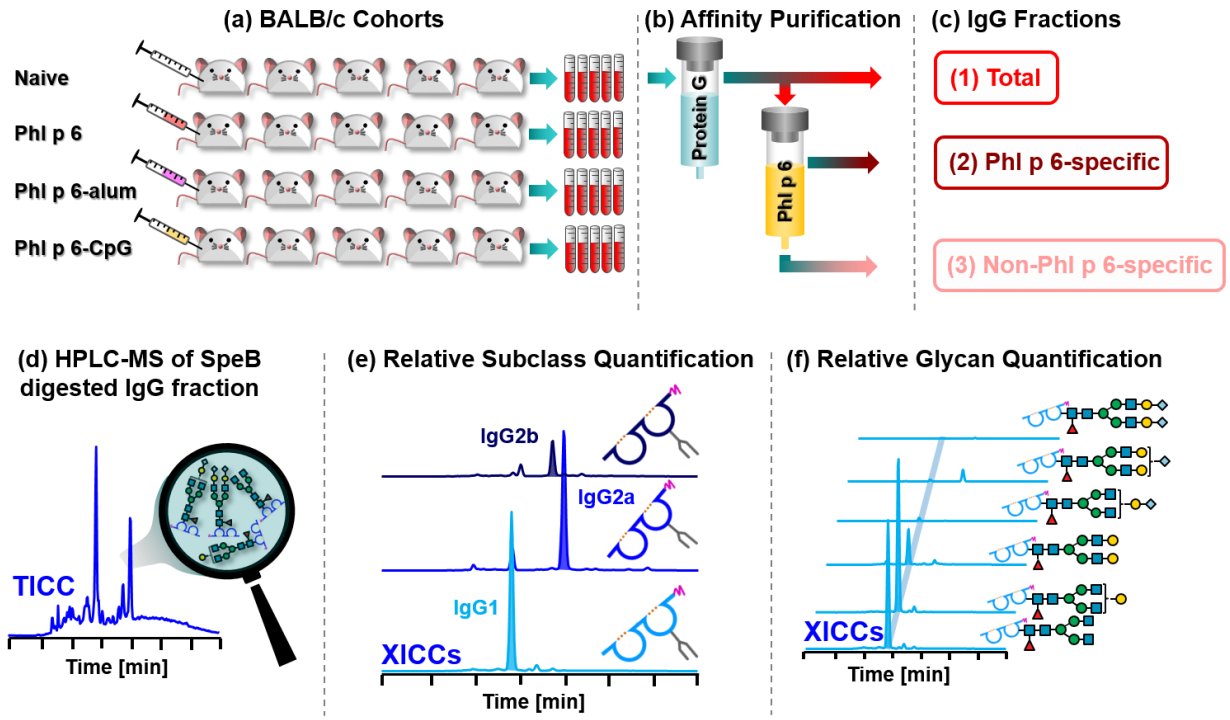

Figure S-9. Schematic workflow of the Phl p 6 vaccination study in BALB/c mice. (a) Serum was obtained from naive mice and mice treated with Phl p 6 in the absence or presence of adjuvants (alum or CpG), respectively (n=5). (b) Polyclonal IgGs of all subclasses were purified by protein G affinity chromatography; antigen-specific IgGs of vaccinated mice were affinity-purified from total IgGs using Phl p 6-sepharose. (c) Three IgG fractions were obtained for each vaccinated mouse individual. (d) SpeB digests of IgG fractions were analysed by means of HPLC-MS. XICCs of glycosylated Fc/2 cleavage products were generated to determine (e) relative subclass abundances and (f) relative *N*-glycoform abundances.

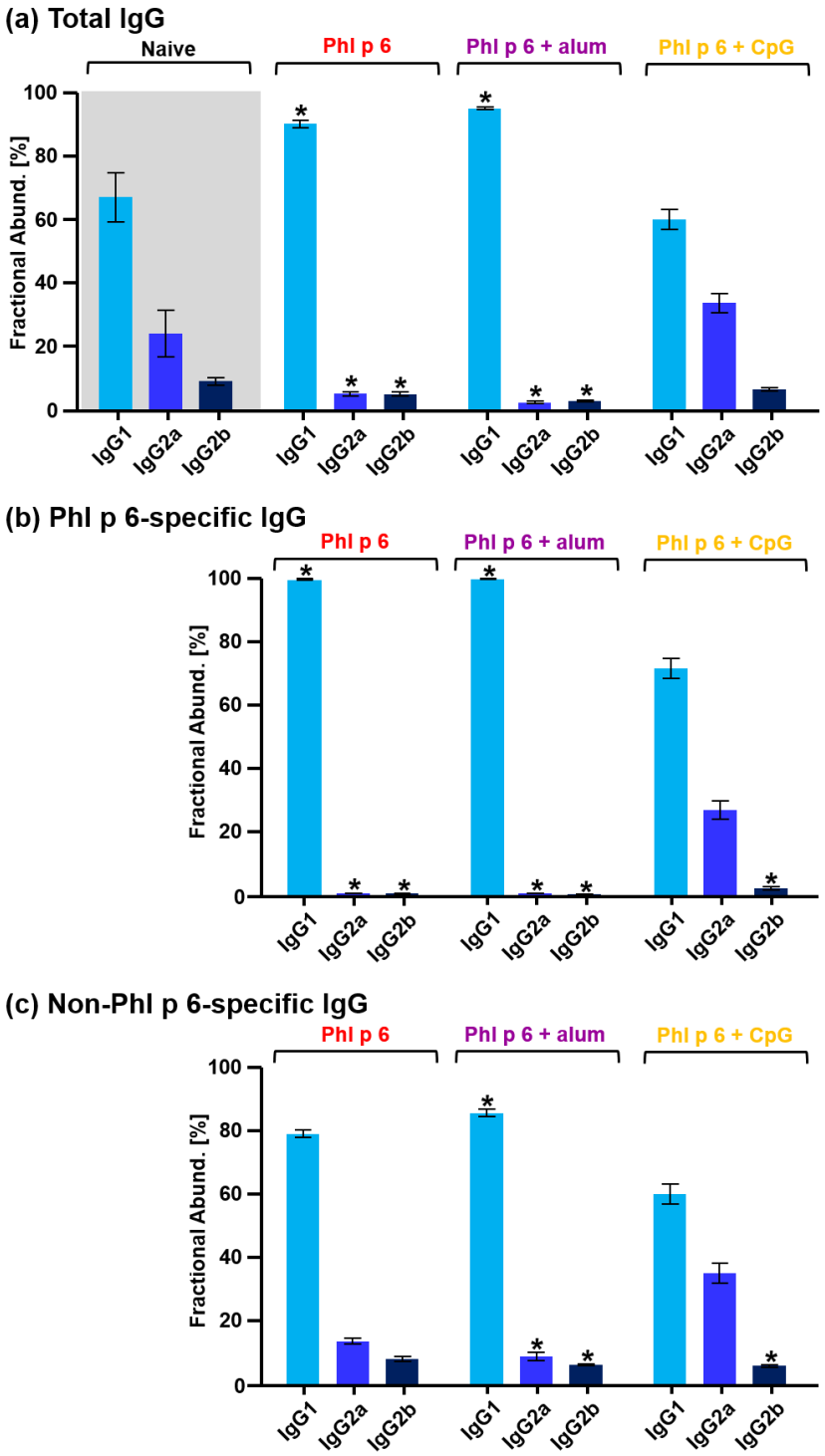

Figure S-10. Fractional abundances of IgG subclasses in (a) total IgG, (b) antigen-specific IgG and (c) antigen-specific depleted IgG from BALB/c mice. Abundances are shown for naive mice and cohorts vaccinated with Phl p 6, Phl p 6 + alum and Phl p 6 + CpG. Relative quantification was based on XICCs of Fc/2 subunits including all detected glycoforms. Mean values of five mouse individuals including standard deviations are shown (n=5) (Supplementary Excel file). Statistical significances were tested using a one-way ANOVA with a Dunnett post-hoc-test using naive mice as a control. Significant changes are indicated with an asterisk ($p \leq 0.05$).

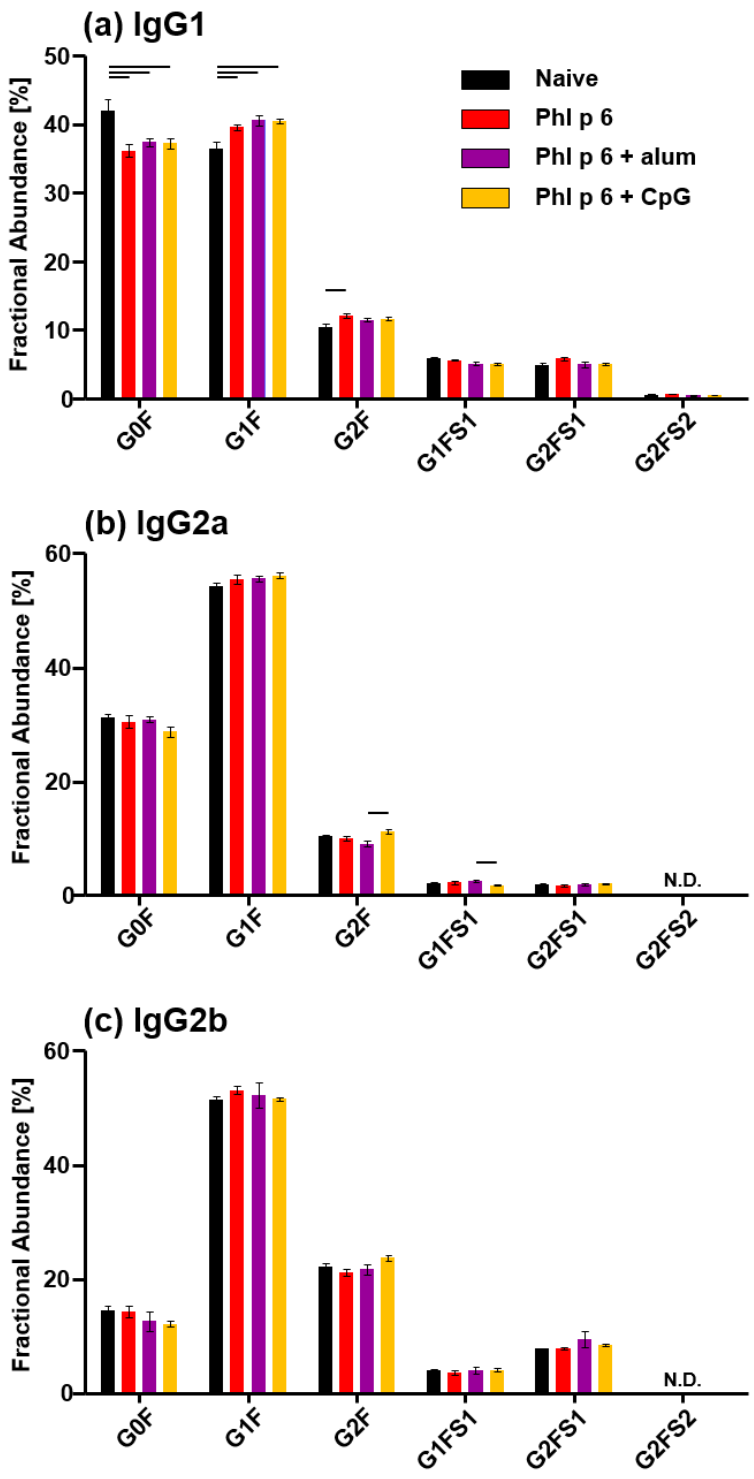

Figure S-11. Subclass-specific glycosylation profiles of total IgGs from naive and Phl p 6-vaccinated BALB/c mice. Relative glycoform abundances of (a) IgG1, (b) IgG2a and (c) IgG2b in naive mice and cohorts treated with Phl p 6, Phl p 6 + alum and Phl p 6 + CpG, respectively, are shown. Fractional abundances represent mean values of five mouse individuals including standard deviations (n=5) (Supplementary Excel file). Statistical significances were tested using a one-way ANOVA with a Tukey post-hoc-test. Significant changes are indicated ($p \leq 0.05$). Note that the abundances of G2F may partially arise from the isobaric αG2F structure comprising α-gal.

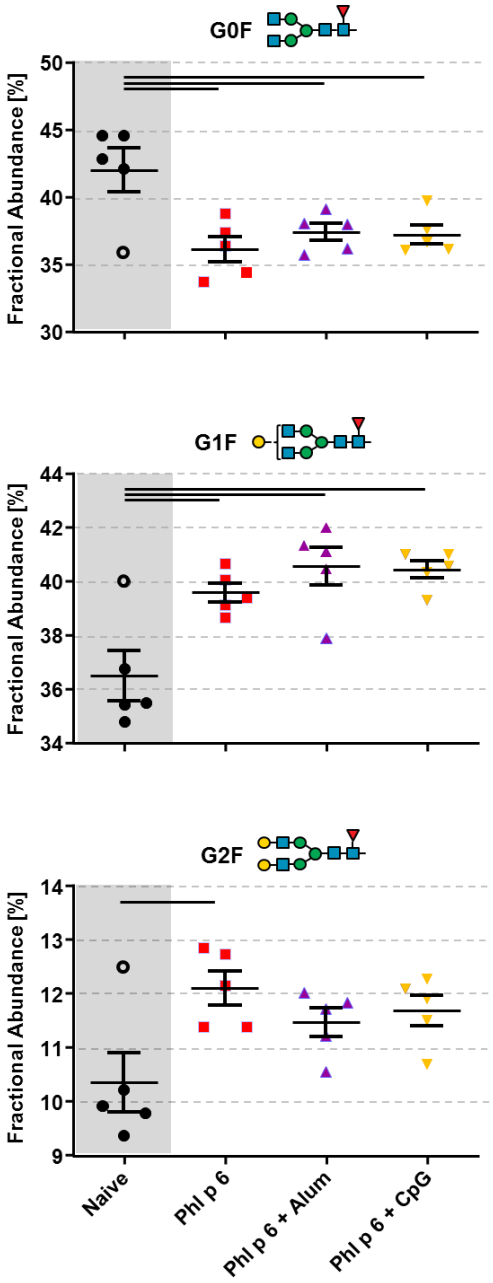

Figure S-12. G0F, G1F and G2F glycoform abundances of IgG1 in total IgGs from naive and Phl p 6-vaccinated BALB/c mouse individuals. Data corresponds to the bar chart shown in Figure S-10 (a). Mean values of five mouse individuals including standard deviations are shown. The outlier individual in the naive cohort is indicated as open circle. Statistical significances were tested using a one-way ANOVA with a Tukey post-hoc-test. Significant changes are indicated ($p \leq 0.05$). Note that the abundances of G2F may partially arise from the isobaric αG2F structure comprising α-gal.

Table S-1. SpeB cleavage products of murine IgG heavy chains from different sources. Main and minor cleavage products are designated Fc/2 and Fc/2*, respectively. Theoretical monoisotopic masses were calculated for G1F *N*-glycoforms lacking the C-terminal lysine residue; intramolecular disulphide bonds were considered to be intact. Experimental masses are mean values of three technical replicates.
[a]Theoretical monoisotopic masses were calculated using GPMAW. [b]Experimental monoisotopic masses were obtained by deconvolution using the Xtract algorithm implemented in the Xcalibur™ software. [c]Standard deviations were calculated from three technical replicates. [d]The low mass accuracy may be attributed to a previously described +1 Da shift arising from an isotopic misassignment during deconvolution.[3]

	Sub-class	Uniprot ID	Product	Amino acids	Fractional abundance [%]	Theoretical mass [Da][a]	Experimental mass [Da][b]	Standard mass deviation [mDa][c]	Mass accuracy [ppm]
BALB/c	IgG1	P01868	Fc/2	110-323	93.04	25,871.57	25,871.50	5.03	-2.58
			Fc/2*	108-323	6.96	26,087.66	26087.87	15.37	3.96
	IgG2a	P01863	Fc/2	112-329	95.30	26,339.87	26,340.85	2.00	37.20[d]
			Fc/2*	117-239	4.70	25,857.68	25,858.71	3.61	39.83[d]
	IgG2b	P01867	Fc/2	117-334	64.28	26,088.91	26,089.87	1.53	36.92[d]
			Fc/2*	116-334	35.72	26,217.00	26,217.01	4.04	0.25
C57BL/6	IgG1i	A0A075B5P4	Fc/2	110-323	96.44	25,836.64	25,836.60	3.61	-1.55
			Fc/2*	108-323	3.56	26,052.73	26,052.74	14.73	0.38
	IgG2bi	A0A075B5P3	Fc/2	118-335	71.69	26,069.97	26,070.98	1.15	38.87[d]
			Fc/2*	117-335	28.31	26,198.06	26,198.05	1.00	-0.38
	IgG2c	A0A0A6YY53	Fc/2	118-334	68.07	25,794.80	25,794.81	5.51	0.52
			Fc/2*	119-334	31.93	25,723.76	25,723.76	0.58	0.00
mAb	IgG3	P03987	Fc/2*	109-329	70.90	26,394.03	26,394.00	8.08	-1.26
			Fc/2	105-329	29.10	26,746.21	26,746.19	1.53	-0.87

Table S-2. *N*-glycan structures considered in glycoform assignment using MoFi software.[4] The library is based on glycopeptide data for murine IgGs reported in recent literature.[5]

Structure	Abbreviation	Elemental composition	Monosaccharide composition	Monoisotopic mass [Da]
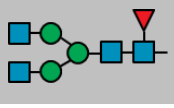	G0F	H92C56N4O39	$HexNAc_4$ Hex_3 Fuc	1444.53387
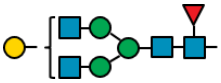	G1F	H102C62N4O44	$HexNAc_4$ Hex_4 Fuc	1606.58669
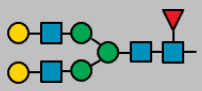 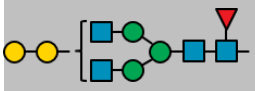	G2F αG2F	H112C68N4O49	$HexNAc_4$ Hex_5 Fuc	1768.63952
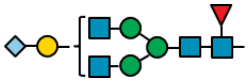	G1FS1	H119C73N5O53	$HexNAc_4$ Hex_4 Fuc Neu5Gc	1913.67702
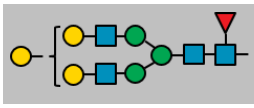	αG3F	H122C74N4O54	$HexNAc_4$ Hex_6 Fuc	1930.69236
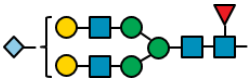	G2FS1	H129C79N5O58	$HexNAc_4$ Hex_5 Fuc Neu5Gc	2075.72985
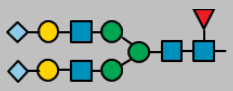	G2FS2	H148C90N6O67	$HexNAc_4$ Hex_5 Fuc $Neu5Gc_2$	2384.83583
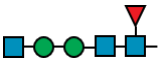		H66C40N2O29	$HexNAc_3$ Hex_2 Fuc	1038.37512
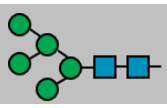		H76C46N2O35	$HexNAc_2$ Hex_5	1216.42286
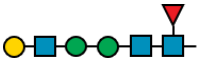 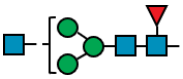		H79C48N3O34	$HexNAc_3$ Hex_3 Fuc	1241.45450
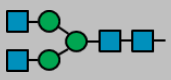	G0	H82C50N4O35	$HexNAc_4$ Hex_3	1298.47596

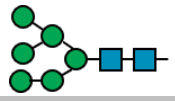		H86C52N2O40	$HexNAc_2$ Hex_6	1378.47569
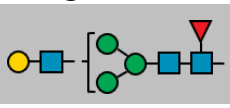		H89C54N3O39	$HexNAc_3$ Hex_4 Fuc	1403.50732
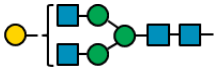	G1	H92C56N4O40	HexNAc4 Hex4	1460.52878
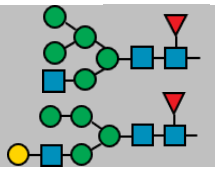		H99C60N3O44	$HexNAc_3$ Hex_5 Fuc	1565.56014
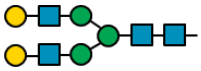	G2	H102C62N4O45	$HexNAc_4$ Hex_5	1622.58161
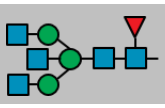		H105C64N5O44	$HexNAc_5$ Hex_3 Fuc	1647.61325
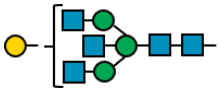		H105C64N5O45	$HexNAc_5$ Hex_4	1663.60816
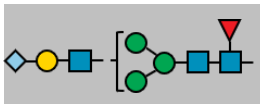		H106C65N4O48	$HexNAc_3$ Hex_4 Fuc Neu5Gc	1710.59765
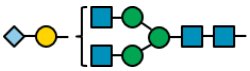		H109C67N5O49	$HexNAc_4$ Hex_4 Neu5Gc	1767.61911
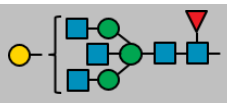		H115C70N5O49	$HexNAc_5$ Hex_6 Fuc	1809.66608
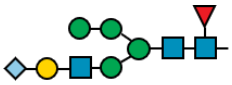		H116C71N4O53	$HexNAc_3$ Hex_5 Fuc Neu5Gc	1872.65047
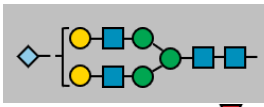		H119C73N5O54	$HexNAc_4$ Hex_5 Neu5Gc	1929.67194
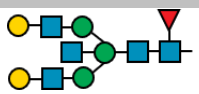		H125C76N5O54	$HexNAc_5$ Hex_5 Fuc	1971.71889
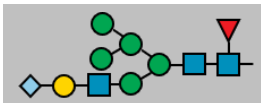		H126C77N4O58	$HexNAc_3$ Hex_6 Fuc $Neu5Gc_1$	2034.70332
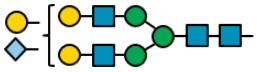		H129C79N5O59	$HexNAc_4$ Hex_6 $Neu5Gc_1$	2091.72476
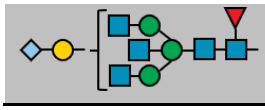		H132C81N6O58	$HexNAc_5$ Hex_4 Fuc Neu5Gc	2116.75640

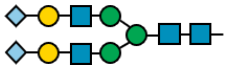	H136C84N6O63	$HexNAc_4$ Hex_5 $Neu5Gc_2$	2236.76227
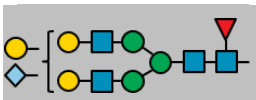	H139C85N5O63	$HexNAc_4$ Hex_6 Fuc $Neu5Gc_1$	2237.78269
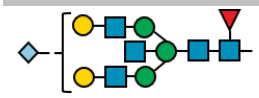	H142C87N6O63	$HexNAc_5$ Hex_5 Fuc Neu5Gc	2278.80922
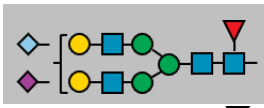	H146C90N6O66	$HexNAc_4$ Hex_5 Fuc Neu5Gc Neu5Ac	2366.82526
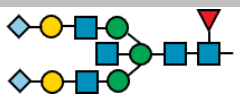	H159C98N7O72	$HexNAc_5$ Hex_5 Fuc $Neu5Gc_2$	2585.89955

SI References

1 Fellers, R. T. *et al.* ProSight Lite: graphical software to analyze top-down mass spectrometry data. *Proteomics* **15**, 1235-1238 (2015).

2 Peri, S., Steen, H. & Pandey, A. GPMAW--a software tool for analyzing proteins and peptides. *Trends Biochem Sci* **26**, 687-689 (2001).

3 Senko, M. W., Beu, S. C. & McLafferty, F. W. Determination of monoisotopic masses and ion populations for large biomolecules from resolved isotopic distributions. *Journal of the American Society for Mass Spectrometry* **6**, 229-233 (1995).

4 Skala, W., Wohlschlager, T., Senn, S., Huber, G. E. & Huber, C. G. MoFi: A Software Tool for Annotating Glycoprotein Mass Spectra by Integrating Hybrid Data from the Intact Protein and Glycopeptide Level. *Anal Chem* **90**, 5728-5736, doi:10.1021/acs.analchem.8b00019 (2018).

5 de Haan, N. *et al.* The N-Glycosylation of Mouse Immunoglobulin G (IgG)-Fragment Crystallizable Differs Between IgG Subclasses and Strains. *Front Immunol* **8**, 608, doi:10.3389/fimmu.2017.00608 (2017).